

THE UNIVERSITY OF MANITOBA

THE LOADING RATE EFFECT ON THE FAILURE
STRENGTH OF GRAY CAST IRON

by

Kee Chung Chao

A THESIS

SUBMITTED TO THE FACULTY OF GRADUATE STUDIES
IN PARTIAL FULFILLMENT OF THE REQUIREMENTS FOR THE
DEGREE OF MASTER OF SCIENCE

DEPARTMENT OF MECHANICAL ENGINEERING

WINNIPEG, MANITOBA

June 1983

THE LOADING RATE EFFECT ON THE FAILURE
STRENGTH OF GRAY CAST IRON

BY

KEE CHUNG CHAO

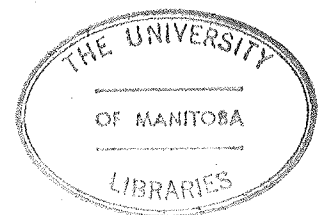
A thesis submitted to the Faculty of Graduate Studies of
the University of Manitoba in partial fulfillment of the requirements
of the degree of

MASTER OF SCIENCE

© 1983

Permission has been granted to the LIBRARY OF THE UNIVERSITY OF MANITOBA to lend or sell copies of this thesis, to the NATIONAL LIBRARY OF CANADA to microfilm this thesis and to lend or sell copies of the film, and UNIVERSITY MICROFILMS to publish an abstract of this thesis.

The author reserves other publication rights, and neither the thesis nor extensive extracts from it may be printed or otherwise reproduced without the author's written permission.



ABSTRACT

The physical and mechanical properties of gray cast iron were studied in this thesis. The main emphasis was placed on the impact properties of the material.

A series of impact tests was carried out to investigate the loading rate effect on the failure strength of gray cast iron. The impact tests were performed on a specially designed instrumented drop weight test machine G20 and G40 specimens with different configurations were tested to failure under varying loading rates.

The validity of the test results was discussed, based on the analysis of the dynamic response of the test system and the frequency response of the load cell to the impact loading.

It was found that gray cast iron is a loading rate sensitive material. The failure strength increases as the loading rate increases. Gray cast iron is also said to be notch insensitive under static and impact loading.

ACKNOWLEDGEMENTS

The author wishes to express his appreciation to the University of Manitoba and particularly to his advisor, Dr. J. Shewchuk, for his guidance.

The help and suggestions from Mr. A. Lohse throughout this research is also gratefully acknowledged.

TABLE OF CONTENTS

Abstract.....	i
Acknowledgement.....	ii
Table of Contents.....	iii
List of Figures.....	vi
List of Tables.....	viii
1. INTRODUCTION	
1.1 Introduction.....	1
1.2 Statement of Problem.....	2
1.3 Scope of Thesis.....	2
2. PROPERTIES OF GRAY CAST IRON	
2.1 Classification of Gray Cast Iron.....	3
2.2 Factors Affecting Properties of Gray Cast Iron.....	4
2.2.1 The Rate of Solidification.....	4
2.2.2 Chemical Composition.....	6
2.3 Physical Properties of Gray Cast Iron.....	7
2.4 Mechanical Properties of Gray Cast Iron.....	11
2.5 Proposed Instrumented Test for Impact Strength Measurement.....	22

3.	EXPERIMENTAL STUDY	
3.1	Introduction.....	23
3.2	Material and Specimens.....	24
3.3	Test Equipment.....	30
3.3.1	Drop Weight Testing Machine.....	30
3.3.2	Load Cell and Anvil Assembly.....	33
3.3.3	Amplifier.....	33
3.3.4	Waveform Recorder.....	37
3.3.5	Strip Chart Recorder.....	37
3.4	Calibration of the Equipment.....	38
3.5	Test Procedure.....	38
3.5.1	Static Tensile Test.....	38
3.5.2	Impact Tensile Test.....	39
4.	TEST RESULTS	
4.1	Results of the Static Tensile Tests.....	40
4.2	Results of the Impact Tensile Tests.....	40
4.2.1	Force-Time Record.....	40
4.2.2	Impact Test Results of G20 Specimens.....	46
4.2.3	Impact Test Results of G40 Specimens.....	46

5.	DISCUSSION AND ANALYSIS	
5.1	Introduction.....	51
5.2	Discussion of the Static Test Results.....	51
5.3	Dynamic Response of the System to Impact Loading.....	52
5.4	The Frequency Response of the Load Cell.....	56
5.5	Discussion of the Impact Test Results.....	57
5.6	Notch, Size and Grade Effect.....	64
6.	CONCLUSIONS	
6.1	Conclusions.....	66
6.2	Suggestions for Further Research.....	66
	LIST OF REFERENCE.....	68
	APPENDIX	
A.	CALIBRATION OF THE TEST EQUIPMENT	
B.	RESPONSE OF A SDOF SYSTEM TO RAMP LOADING	

LIST OF FIGURES

[1]	Relation Between Poisson's Ratio and Tensile Stress of G30 Gray Iron.....	9
[2]	Relation Between Poisson's Ratio and Compressive Stress of G30 Gray Iron.....	10
[3]	Damping of Three Materials.....	10
[4]	Stress-Strain Curves of 3 Grades of Gray Iron in Tension.....	13
[5]	Relation Between Tensile and Compressive Strength of Gray Iron.....	14
[6]	Schematic Diagram of Transverse Test of Gray Castings.....	15
[7]	Relation Between Hardness and Strength.....	17
[8]	Relation Between Impact Strength of Gray Iron and its Transverse resilience as Calculated from the Breaking Load and the Deflection in the Transverse Strength Test.....	19, 20
[9]	Tensile Specimen of Gray Cast Iron.....	26
[10]	Schematic Diagram of the Instrumentation for the Instrumented Drop-Weight Test.....	31
[11]	Drop-Weight Testing Machine and Measurement Instruments.....	32
[12]	Load cell and Specimen.....	34
[13]	Schematic Diagram of Wheatstone Bridge Circuit...	35
[14]	Anvil Assembly and Drop-Weight.....	36
[15][16]	Typical Force-Time Records of Impact Test from Strip Chart Recorder.....	43, 44
[17]	Typical Force-Time Records of Impact Test from Oscilloscope.....	45
[18]	Schematic Diagram of the Equivalent Cross Bars-Specimen System.....	53
[19]	Response of SDOF System to Ramp Impulse.....	55
[20]	Relation Between Impact Velocity and Loading Time.....	58

[21]	Loading Rate Effect on the Failure Stress of G20 Specimens.....	61
[22]	Loading Rate Effect on the Failure Stress of G40 Specimens.....	62
[23]	Calibrated F- ϵ Relation of Load Cell.....	71

LIST OF TABLES

[1]	Classification of Gray Cast Iron.....	3
[2]	Typical Compositions of Gray Cast Iron Based on Strength and Section.....	5
[3]	Impact Properties of Gray Iron Test Bar.....	19
[4]	Test Program.....	24
[5]	Chemical Composition of Test Materials Provided by the Foundry.....	25
[6]	Static Test Results of G20 Specimens.....	41
[7]	Static Test Results of G40 Specimens.....	42
[8]	Impact Test Results of Unnotched G20 Specimens...	47
[9]	Impact Test Results of Notched G20 Specimens.....	48
[10]	Impact Test Results of Unnotched G40 Specimens...	49
[11]	Impact Test Results of Notched G40 Specimens.....	50

CHAPTER 1
INTRODUCTION

1.1 Introduction

Gray cast iron is a structural material which has been used for many centuries. In spite of the rapid development of new materials, gray cast iron is still widely used. It is one of our most important materials from the standpoint of its low cost, good castability and machinability. Typical applications are engine blocks, heads; bases, frames, beds and supports for machine tools.

Gray cast iron has considerably lower impact strength than either steel or malleable iron. However, in many gray iron castings, some impact strength is important for the resistance to breakage. There is incomplete agreement on a standard impact test method for cast iron. ASTM standard A327 recommends Charpy type impact tests with unnotched bar specimen for gray cast irons and notched bar specimen for malleable irons. The usefulness of this kind of impact tests is limited, because the test results determine only the relative difference in failure strength of the materials.

In the past few years, as a result of development of stress measuring techniques, considerable progress has been made in measurement and analysis of dynamic stresses. Instrumented impact tests, which provide load-time

information in addition to the energy absorbed, have been introduced to study the dynamic properties of materials. The load and time to failure, as well as the area under the load-time curve corresponding to the energy absorbed can be obtained from the tests.

1.2 Statement of Problem

This thesis is mainly an experimental study of the impact strength of gray cast iron under varying loading rates. The effect of size and geometry of specimen on the impact strength is also investigated.

1.3 Scope of Thesis

The thesis is divided into six chapters. Chapter 2 of the thesis deals with a literature survey of the properties of gray cast iron. Mechanical, physical and other related properties are included, with particular emphasis on impact properties.

The experimental study, including the test program, test equipment, and test procedure is described in Chapter 3, with results and discussions appearing in Chapter 4 and 5.

The final chapter is devoted to the conclusion and suggestions for further work.

A list of references and an appendix is presented at the end of the thesis. The appendix contains the procedure for calibration and a mathematical solution of ramp impulse to SDOF system.

CHAPTER 2

PROPERTIES OF GRAY CAST IRON

2.1 Classification of Gray Cast Iron

Gray cast iron is an alloy of iron, carbon and silicon, in which more carbon is present than can be retained in solid solution in austenite at the eutectic temperature. A simple and convenient classification of gray cast iron can be found in ASTM A48^[1] which relates the various types in terms of tensile strength. This classification is shown in Table 1, where the first three classes cover the ordinary grades and remainders are considered high-strength gray cast iron.

TABLE 1 CLASSIFICATION OF G.C.I.

<u>CLASS</u>	<u>T.S. MIN (lb/IN²)</u>
G20	20,000
G25	25,000
G30	30,000
G35	35,000
G40	40,000
G50	50,000
G60	60,000

The ASTM classification by no means connotes a scale of ascending superiority from class G20 to G60, because in many applications, strength is not the major criterion for the choice of grade.

Table 2 gives typical compositions to meet the various classes of ASTM A48 specification. The values in this table are only suggestions and not a part of the specification, but they have been checked against successful practice. [3] It should be noted that increased strength is obtained by progressively lowering the carbon and silicon contents.

Analyses of gray cast iron usually fall within the following limits: Total carbon 2.5 - 3.5 percent; combined carbon 0.6 - 0.9 percent; silicon 1.5 - 3 percent; and phosphorus 0.2 percent.

Specific properties of gray cast iron may be modified by the use of alloying elements such as nickel, chromium, molybdenum, vanadium and copper.

2.2 Factors Affecting Properties of Gray Cast Iron

The structure and properties of gray cast iron are affected by the following factors.

2.2.1 The Rate of Solidification

Slow rates of solidification allow for graphite formation, and castings made in sand molds tend to form a casting which is soft and machinable. More rapid solidification will tend to prevent the formation of graphite, and give a white iron casting which is hard

Type	Composition, %					Average carbon equivalent(a)	Metal section range, in.	Brinell hardness number	Transverse load, lb	Transverse deflection, in.	Tensile strength, psi
	TC	Si	P	S	Mn						
Class 20, light section, 0.875-in. test bar	3.50	2.40	0.20	0.08	0.50	4.56	Up	160	900	0.10	22,000
to to to to to	to	to	to	to	to	...	to	to	to	to	to
0.875-in. test bar	3.80	2.60	0.80	0.13	0.70	...	0.50	200	1200	0.15	26,000
Class 20, medium section, 1.2-in. test bar	3.40	2.30	0.20	0.08	...	4.34	1/2	160	1600	0.20	18,000
to to to to to	to	to	to	to	to	to	to	to	to
1.2-in. test bar	3.60	2.50	0.60	0.80	1	180	2200	0.27	24,000
Class 20, heavy section, 2.0-in. test bar	3.10	2.20	0.20	0.08	0.50	3.98	1	130	4500	...	18,000
to to to to to	to	to	to	to	to	...	and	to	to	...	to
2.0-in. test bar	3.30	2.40	0.40	0.13	0.80	...	up	180	6500	...	22,000
Class 25, light section, 0.875-in. test bar	3.30	2.20	0.20	0.08	0.50	4.20	Up	160	950	0.11	26,000
to to to to to	to	to	to	to	to	...	to	to	to	to	to
0.875-in. test bar	3.50	2.40	0.50	0.13	0.80	...	1/2	180	1300	0.16	29,000
Class 25, medium section, 1.2-in. test bar	3.20	2.20	0.15	0.08	0.50	4.08	1/2	172	1800	0.22	26,000
to to to to to	to	to	to	to	to	...	to	to	to	to	to
1.2-in. test bar	3.40	2.40	0.40	0.12	0.80	...	1	207	2400	0.28	29,000
Class 25, heavy section, 2.0-in. test bar	3.00	1.90	0.15	0.08	0.50	3.82	1	179	6000	...	26,000
to to to to to	to	to	to	to	to	...	and	to	to	...	to
2.0-in. test bar	3.30	2.20	0.25	0.12	0.80	...	up	217	7800	...	30,000
Class 30, light section, 0.875-in. test bar	3.20	2.10	0.15	0.08	0.50	4.03	1/2	179	1250	...	30,000
to to to to to	to	to	to	to	to	...	to	to	to	...	to
0.875-in. test bar	3.40	2.30	0.30	0.12	0.80	...	1	228	1500	...	34,500
Class 30, medium section, 1.2-in. test bar	3.10	2.10	0.15	3.92
to to to to to	to	to	to
1.2-in. test bar	3.30	2.30	0.25
Class 30, heavy section, 2.0-in. test bar	2.90	1.70	0.15	0.08	0.45	3.68	1	207	6500	...	30,000
to to to to to	to	to	to	to	to	...	and	to	to	...	to
2.0-in. test bar	3.20	2.10	0.25	0.12	0.70	...	up	228	8200	...	34,500
Class 35, light section, 0.875-in. test bar	3.10	2.00	0.15	0.08	0.45	3.90	...	179	1150	...	36,000
to to to to to	to	to	to	to	to	...	to	to	to	...	to
0.875-in. test bar	3.30	2.20	0.30	0.12	0.70	...	1/2	228	1450	...	40,000
Class 35, medium section, 1.2-in. test bar	3.00	1.80	0.15	0.07	0.46	3.77	1/2	207	2300	0.25	35,000
to to to to to	to	to	to	to	to	...	to	to	to	to	to
1.2-in. test bar	3.25	2.10	0.25	0.12	0.70	...	1	228	3000	0.35	39,000
Class 35, heavy section, 2.0-in. test bar	2.80	1.60	0.10	0.06	0.45	3.54	1	183	7500	0.32	35,000
to to to to to	to	to	to	to	to	...	and	to	to	to	to
2.0-in. test bar	3.10	2.00	0.20	0.12	0.70	...	up	217	9000	0.38	38,000
Class 40, light section, 0.875-in. test bar	3.00	1.90	0.10	0.07	0.45	3.77	...	212	1275	...	42,000
to to to to to	to	to	to	to	to	...	to	to	to	...	to
0.875-in. test bar	3.20	2.20	0.25	0.12	0.65	...	1/2	241	1550	...	46,000
Class 40, medium section, 1.2-in. test bar	2.95	1.70	0.10	0.06	0.45	3.65	1/2	207	2500	0.25	40,000
to to to to to	to	to	to	to	to	...	to	to	to	to	to
1.2-in. test bar	3.15	2.00	0.20	0.11	0.70	...	1	241	3400	0.35	47,000
Class 40, heavy section, 2.0-in. test bar	2.75	1.50	0.07	0.05	0.50	3.42	1	180	8400	0.30	41,000
to to to to to	to	to	to	to	to	...	and	to	to	to	to
2.0-in. test bar	3.00	1.90	0.15	0.12	0.70	...	up	217	9800	0.38	45,000
Class 50, light section, 0.875-in. test bar	2.90	1.70	0.10	0.06	0.50	3.62	...	228	1600	...	51,000
to to to to to	to	to	to	to	to	...	to	to	to	...	to
0.875-in. test bar	3.10	2.10	0.20	0.12	0.70	...	1/2	269	1800	...	55,000
Class 50, medium section, 1.2-in. test bar	2.70	1.70	0.10	0.06	0.60	3.45	1/2	228	3000	0.28	50,000
to to to to to	to	to	to	to	to	...	to	to	to	to	to
1.2-in. test bar	3.00	2.00	0.20	0.11	0.80	...	1	269	4000	0.34	57,000
Class 50, heavy section, 2.0-in. test bar	2.55	1.40	0.07	0.06	0.60	3.20	1	207	10,000	0.38	50,000
to to to to to	to	to	to	to	to	...	and	to	to	to	to
2.0-in. test bar	2.85	1.70	0.15	0.11	0.80	...	up	241	12,500	0.48	54,000
Class 60, light section, 0.875-in. test bar	2.70	1.90	0.10	0.06	0.50	3.51	...	228	1750	...	60,000
to to to to to	to	to	to	to	to	...	to	to	to	...	to
0.875-in. test bar	3.00	2.20	0.20	0.12	0.70	272	2000	...	65,000
Class 60, medium section, 1.2-in. test bar	2.50	1.90	0.05	0.05	0.70	3.37	...	248	3400	0.25	60,000
to to to to to	to	to	to	to	to	...	to	to	to	to	to
1.2-in. test bar	2.85	2.10	0.15	0.10	1.00	290	4500	0.40	65,000
Class 60, heavy section, 2.0-in. test bar	2.50	1.20	0.07	0.05	0.50	3.09	...	212	11,500	0.35	60,000
to to to to to	to	to	to	to	to	...	to	to	to	to	to
2.0-in. test bar	2.80	1.50	0.15	0.12	0.80	248	13,500	0.50	64,000

(a) "Carbon equivalent" is calculated as percentage carbon plus 0.3 times the sum of percentage silicon and phosphorus. Some use carbon plus 1/3 silicon. Data in this table from "Handbook of Cupola Operation", AFS, 1946.

Table 2 Typical Composition of Gray Iron Based on Strength and Section

and less readily machinable. It is also noted that tensile strength tends to increase with higher rate of solidification.

2.2.2 Chemical Composition

Carbon Content The higher the carbon content of the gray cast iron, the lower will be its melting point. Hence, the formation of gray and soft iron tends to occur.

Silicon. Silicon slightly strengthens the ferrite but increases the brittle transition temperature. Indirectly, however, it acts as a softener by increasing the tendency of the formation of cementite separate the graphite and ferrite. High silicon contents increase the acid-corrosion resistance of gray cast iron, which is useful in chemical industries.

Sulphur and Manganese Sulphur is usually present in amounts from 0.03 to 0.07 percent and is a normal constituent of cast iron. The chief function of manganese in gray cast iron is to neutralize the sulphur content by forming manganese sulphide and prevent the formation of the more harmful iron sulphide which tends to stabilize the cementite producing a hard and brittle casting.

Nickel, Chromium, and Molybdenum Alloying elements may be added to gray cast iron in order to improve their properties. For the production of high strength irons,

additions of nickel, chromium and molybdenum are commonly used. Nickel can be a very effective graphitizer to impart more uniform characteristics in variable sections of castings. It also tends to reduce the size of the graphite flakes, thus improving the strength of casting significantly. Chromium promotes the formation of combined carbon. The combination of chromium, nickel and molybdenum produces an iron which is fine-grained and higher in strength, with the graphite uniformly dispersed.

2.3 Physical Properties of Gray Cast Iron

The most significant physical properties of gray cast iron are density, thermal conductivity, coefficient of thermal expansion, electrical properties, Poisson's ratio and damping capacity.

Density Density of gray irons at room temperature varies from 6.95 g/cm^3 to 7.35 g/cm^3 . The density of liquid cast irons just above the final solidification temperature is about 6.23 g/cm^3 . [3]

Thermal Conductivity Thermal Conductivity of gray cast iron at room temperature is approximately the same as of many other ferrous materials, ranging from $0.11 - 0.137$ cal per cm per $^{\circ}\text{C}$ per sec.

Coefficient of thermal expansion Coefficient of thermal expansion of gray cast irons in the range from 0° to 500°C (32° to 932°F) is about 13×10^{-6} per °C. However, at room temperature the commonly used figure of 10×10^{-6} per °C is accurate enough for engineering purposes.

Electrical Properties The specific electrical resistance (resistivity) of gray cast iron, as compared with that of other ferrous metals, is relatively high, apparently because of the amount and distribution of the graphite content. Increases in total carbon content and in silicon content increases resistivity. The resistivity of gray cast iron lies between 75 and 100 microhm/cm, depending on the temperature.

Poisson's Ratio The ratio of elastic lateral strain across a bar to the elastic longitudinal strain is known as Poisson's ratio. Unlike most elastic materials in which the Poisson's ratios are constants, gray cast irons may have varying Poisson's ratio with varying stress and strain. Gilbert^[4] has studied in detail the change of Poisson's ratio with the variation of stress on a typical engineering gray cast iron of 30,000 psi in tensile strength. His results, summarized in Fig. 1 and Fig. 2, show that at low stresses a value of 0.25 is found, decreasing to about 0.22 at a tensile stress of 9,000 psi which is the normal maximum likely to be used

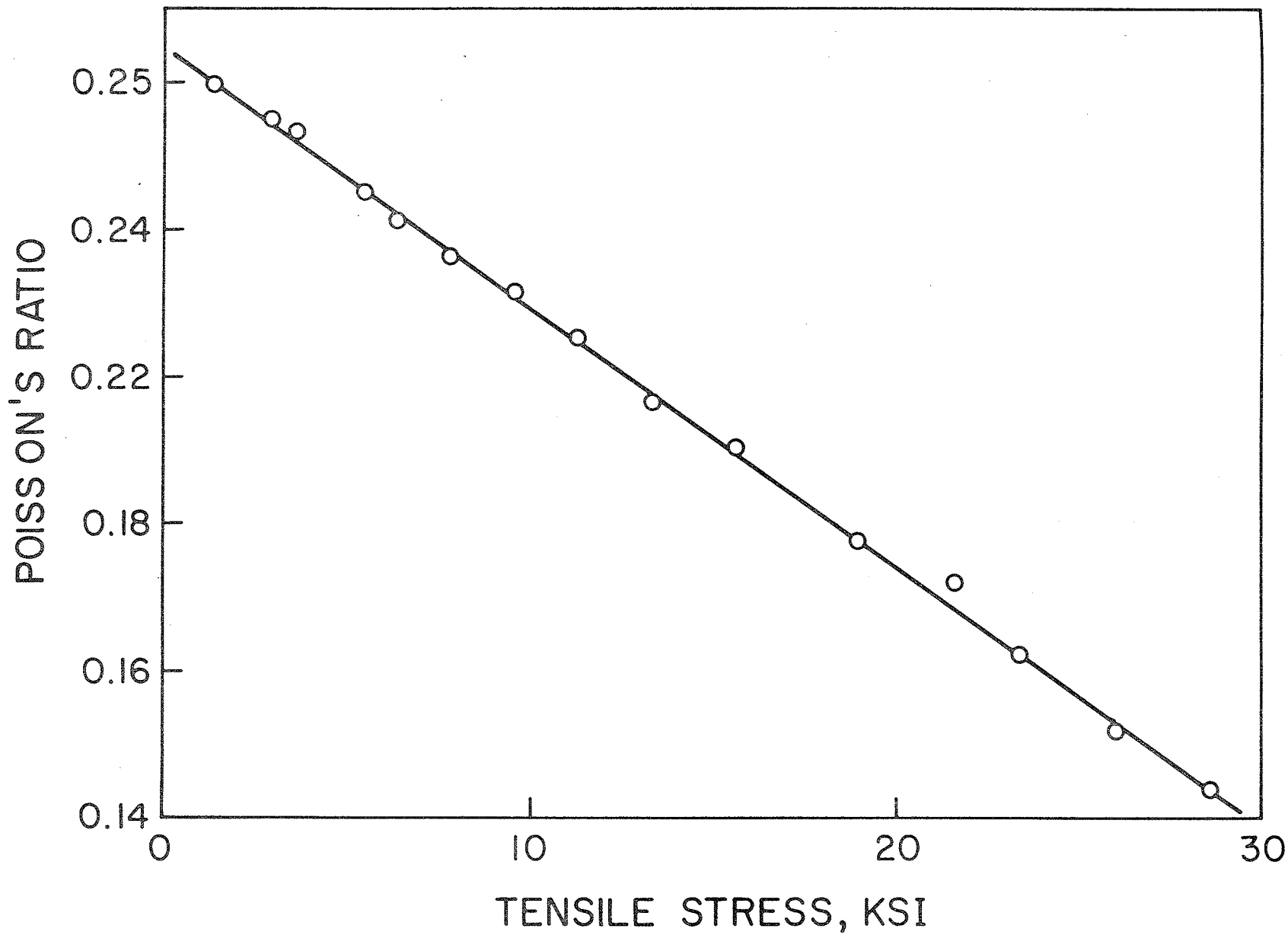


Fig. 1^[4] The Relation Between Poisson's Ratio and Tensile Stress of G30 Gray Iron

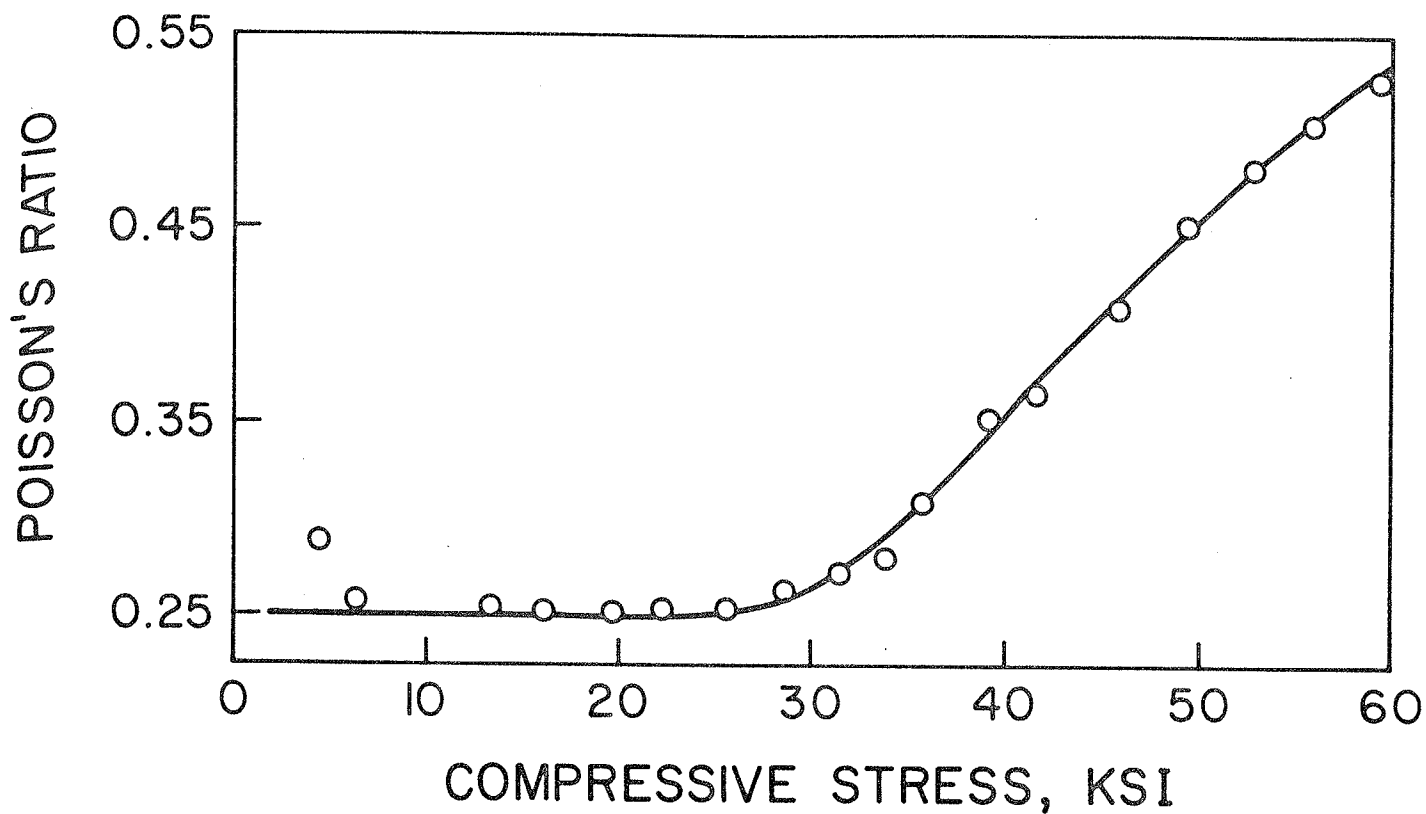


Fig. 2 The Relation Between Poisson's Ratio and Compressive Stress of G30 Gray Iron

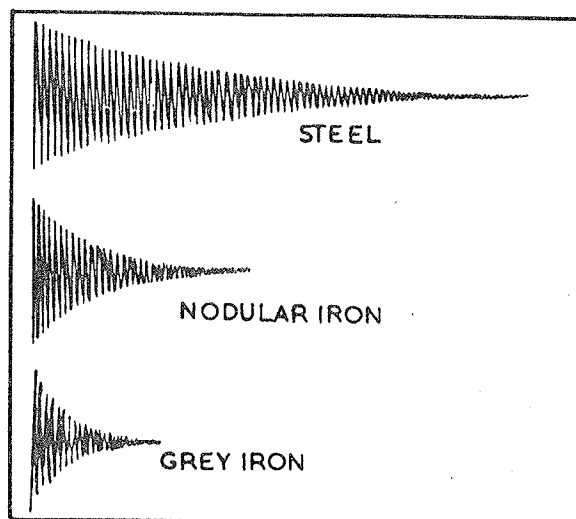


Fig. 3 Damping of Three Materials

in practice. For compressive stresses the value remains substantially constant at 0.25 until the stress exceeds about 27,000 psi, at which point the value increases sharply.

Damping Capacity Damping capacity is the property which permits a material to absorb vibrational stress and energy within the body of the material itself. Gray iron has an exceptionally high damping capacity. A comparison of damping capacities of three materials is shown in Fig. 3.^[4] Gray cast irons have been recognized as excellent materials for parts which have to withstand excessive vibration, (but not impact).

2.4 Mechanical Properties

Gray cast iron is tested to determine its mechanical properties by ascertaining its tensile strength and its transverse modulus of rupture. Compression and hardness tests are sometime used to give additional information. The usefulness of the impact test for gray cast iron is not well established, though a lot of research work has been done in recent years.

Tensile strength Tensile strength is the stress required to fracture test piece by an axially applied load. It is generally determined by the conventional static tensile test. Typical stress-strain curves of gray

cast iron of tensile tests are shown in Fig. 4.^[4] A significant variation in the representative section of the casting should always be considered, since gray cast iron is essentially a non-homogeneous material.

Compressive strength Gray cast iron has a relatively high compressive strength, varying from 80 KSI to approximate 170 KSI. The relationship between compressive strength and tensile strength is linear on a log-log plot, as shown in Fig. 5.

Modulus of elasticity From typical stress-strain curves shown in Fig. 4, it is evident that gray cast iron does not obey Hooke's law. The non-linear characteristic is due mainly to the number and size of graphite flakes. The modulus of elasticity is usually determined from the elongation of the specimen during a tensile test, and is calculated on a load not greater than a quarter of the ultimate breaking load of the test piece. The modulus of gray iron varies from 10×10^6 psi to 23×10^6 psi.

Transverse strength When an as-cast test bar is loaded as a simple beam, as shown in Fig. 6, and the load and deflection required to break it are determined, the resulting value is converted into a nominal index of strength by using the standard beam formula. The value so determined is called the "modulus of rupture", which is an useful parameter for production control, but cannot be used in the design of castings without further analysis and interpretation.

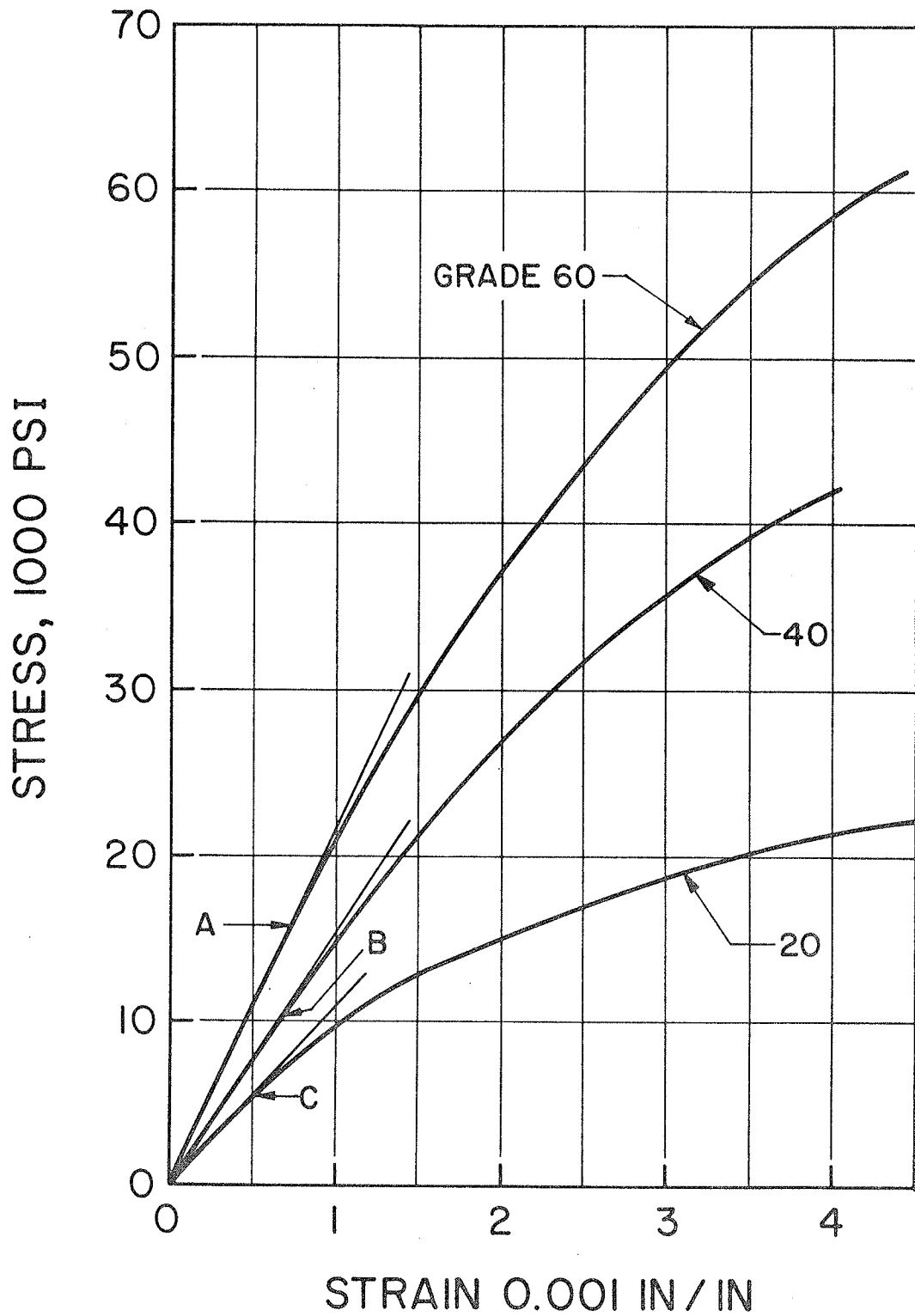
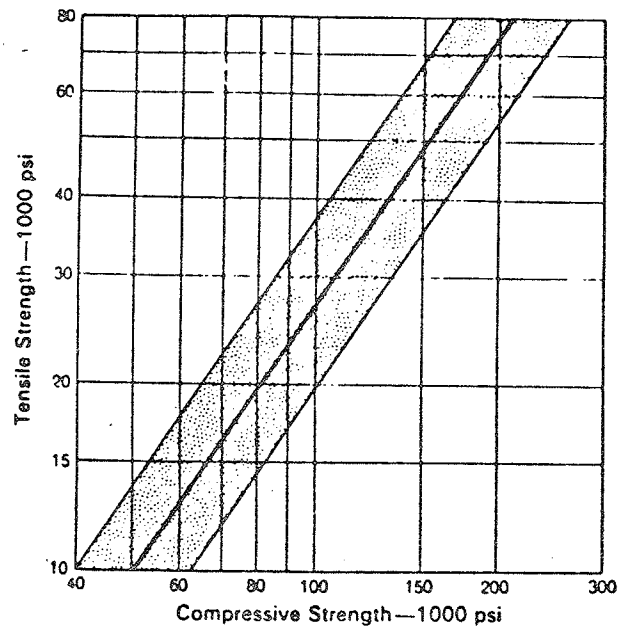
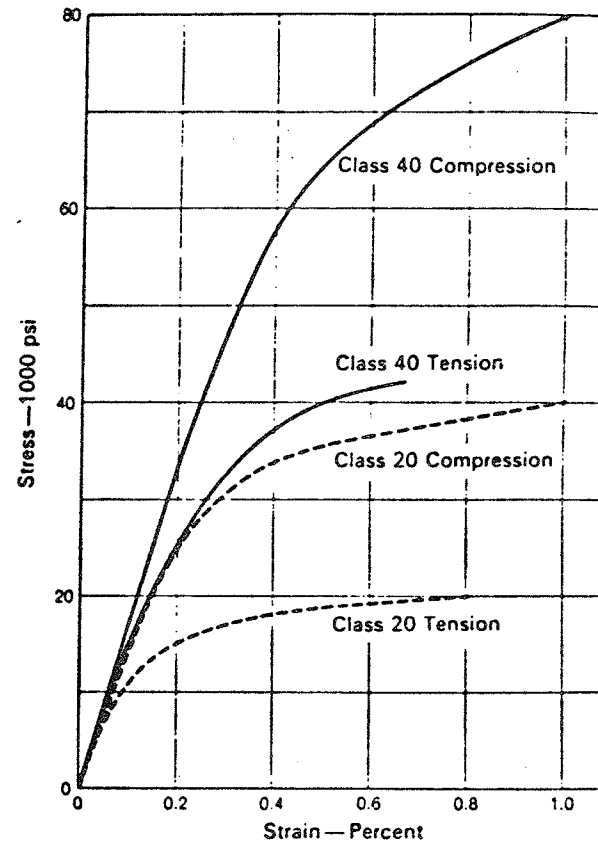


Fig. 4 Stress-Strain Curves of 3 Grades of Gray Iron in Tension. Modulus of Elasticity is Measured to Points A, B, C. Representing 1/4 of the Tensile Strength.



(A)

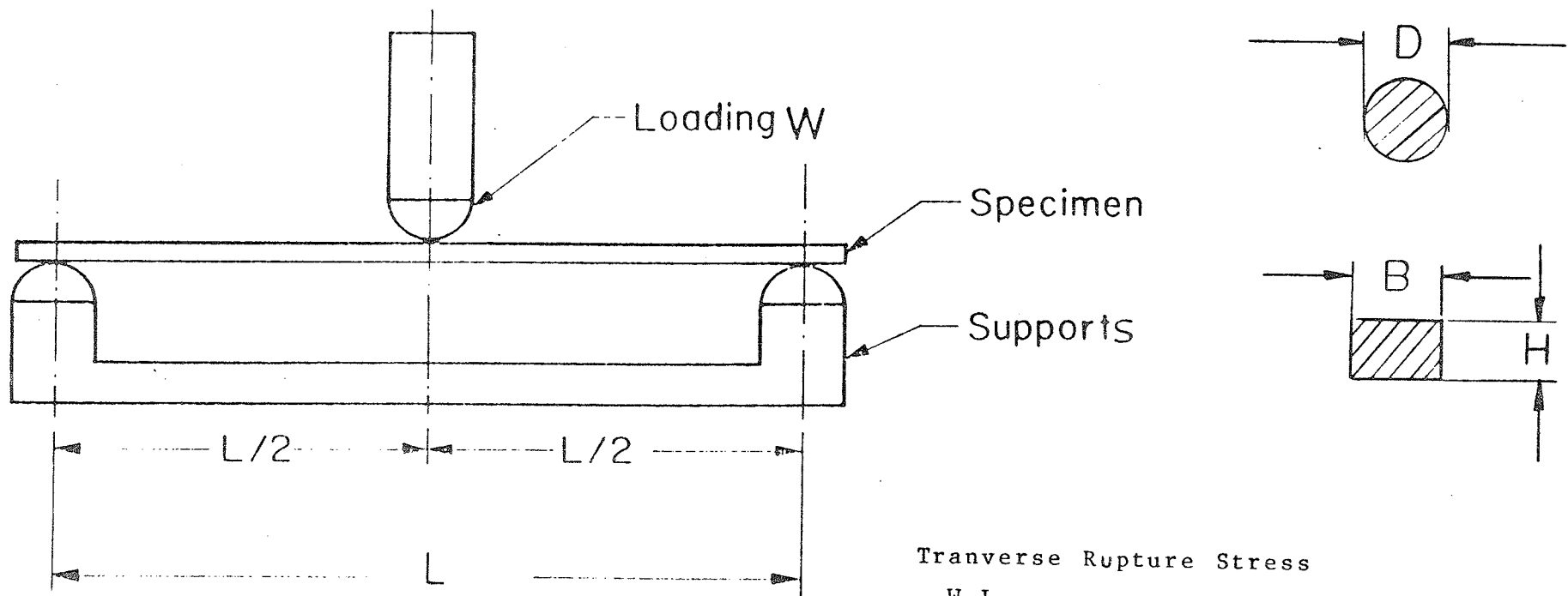
The General Relation Between
Tensile and Compressive Strength
of Gray Iron [6]



(B)

Comparison of Stress-Strain Curves
in Tension and Compression of
G20 and G40 Gray Iron [6]

Fig. 5 Tensile and Compressive Strength of Gray Iron



Transverse Rupture Stress

$$\frac{W_r L}{0.3928 D^3} \quad \text{for Round Bars}$$

$$\frac{3 W_r L}{2 B H^2} \quad \text{for Rectangular Bars}$$

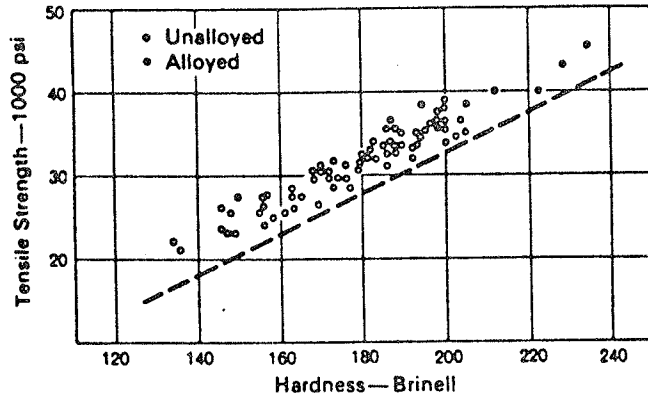
(W_r - Fracture Load)

Fig. 6 Schematic Set-up of Transverse Test

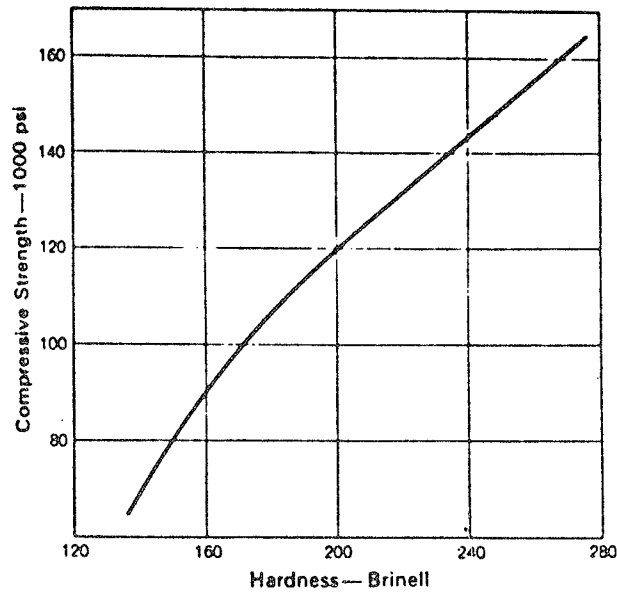
The transverse rupture stress calculated by the standard beam formula is always 1.6 ~ 2.1 times higher than the tensile strength, mainly due to the nonlinear behaviour of gray cast iron. [4]

Hardness The Brinell hardness numbers of gray cast iron are in the range 155 to 320. The relation between Brinell hardness and strength is shown in Fig. 7.

Impact Strength Impact testing has long been in use for the investigation of structural materials, usually by means of transverse test pieces. The energy required to load the specimen to destruction is usually regarded as impact strength. In most ductile materials, impact tests are used to detect dangerous conditions of embrittlement which would not be observed in a normal tensile test. The ordinary impact tests, such as the notched-bar Charpy test and drop weight tear test, are most meaningful when conducted over a range of temperatures so that the temperature at which the ductile-to-brittle transition takes place can be determined. However, the usefulness of an impact test of gray cast iron is not the same as that for ductile materials. Failure of gray cast iron occurs before any general plastic deformation of the matrix takes place and gray cast iron invariably fails in a brittle way. There is no ductile-brittle transition of gray cast iron under impact loading. Gilbert [5] states as follows: "The purpose of an impact test on flake-graphic cast iron



(A)



(B)

Fig. 7 Relation Between Hardness and Strength of Gray Iron

is to obtain an energy value representative of the work done to cause failure. This is referred to as the resilience of the material".

Table 3^[7] provides some values of impact strength in terms of energy of gray cast iron for different grades. The relation between the values of impact fracture energy and resilience as calculated from the load-deflection curves in transverse strength test was studied by various researchers. Fig. 8A and Fig. 8B show the experimental results obtained by Walton^[3] and Gilbert^[5]. It can be observed that all the fracture energies obtained from the impact tests are in excess of the resilience obtained in the slow bend tests. The difference in the values was thought to be mainly due to the energy loss incurred in the impact test as the broken halves of the test piece vibrate between the hammer and anvil.

In addition, Gilbert^[5] carried out Charpy tests using hammers of varying weight and constant impact velocity. It was found that the fracture energy was smaller for the smaller weight of the hammer. He also carried out Charpy tests with constant initial energy and varying impact velocity by using a specific combination of height and weight of the drops. The recorded fracture energy increased as the impact velocity increased.

Impact Strength (ft - lb)	Grades 20, 25	Grades 30, 35	Grades 40, 45	Grades 50, 55
Charpy, unnotched	55	60	70, 80	115, -
Izod, unnotched	21, 22	23, 25	31, 35	75, 120

Table 3 Impact Properties of Gray Iron Test Bar as Cast [7]

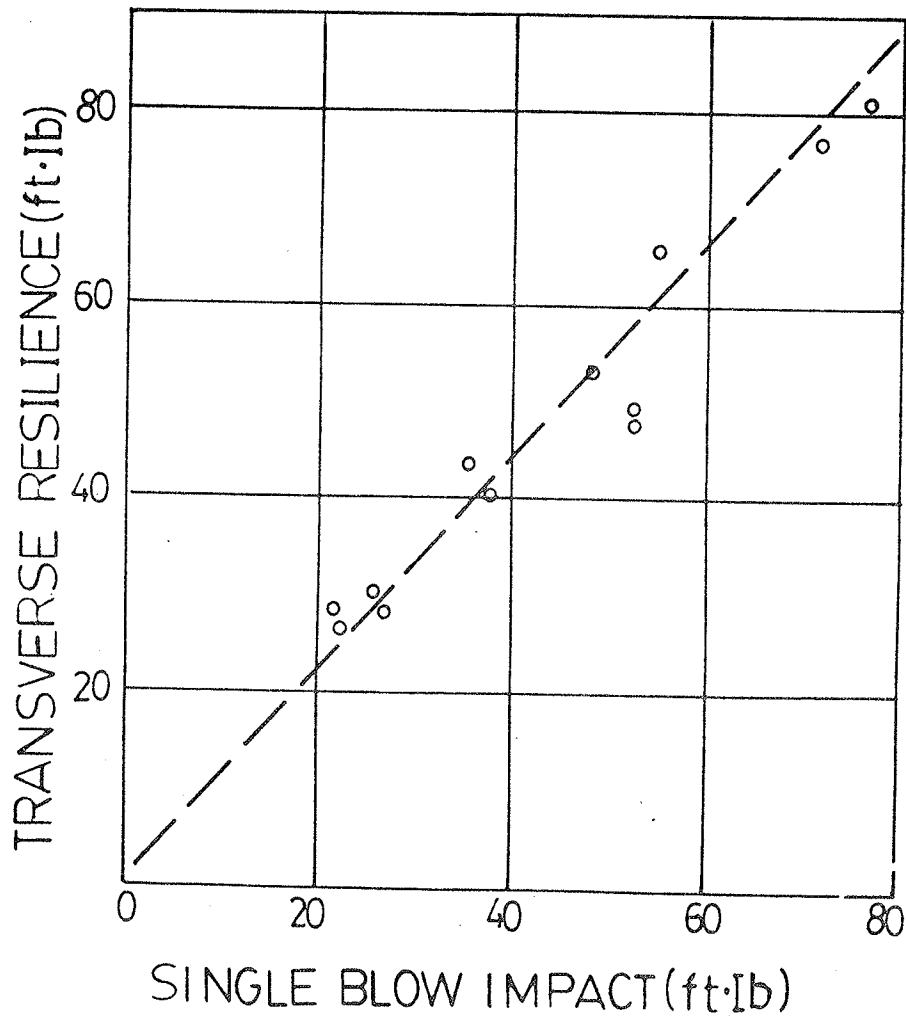


Fig. 8A The Relation Between Impact Strength, of Gray Iron and Its Transverse Resilience [3]

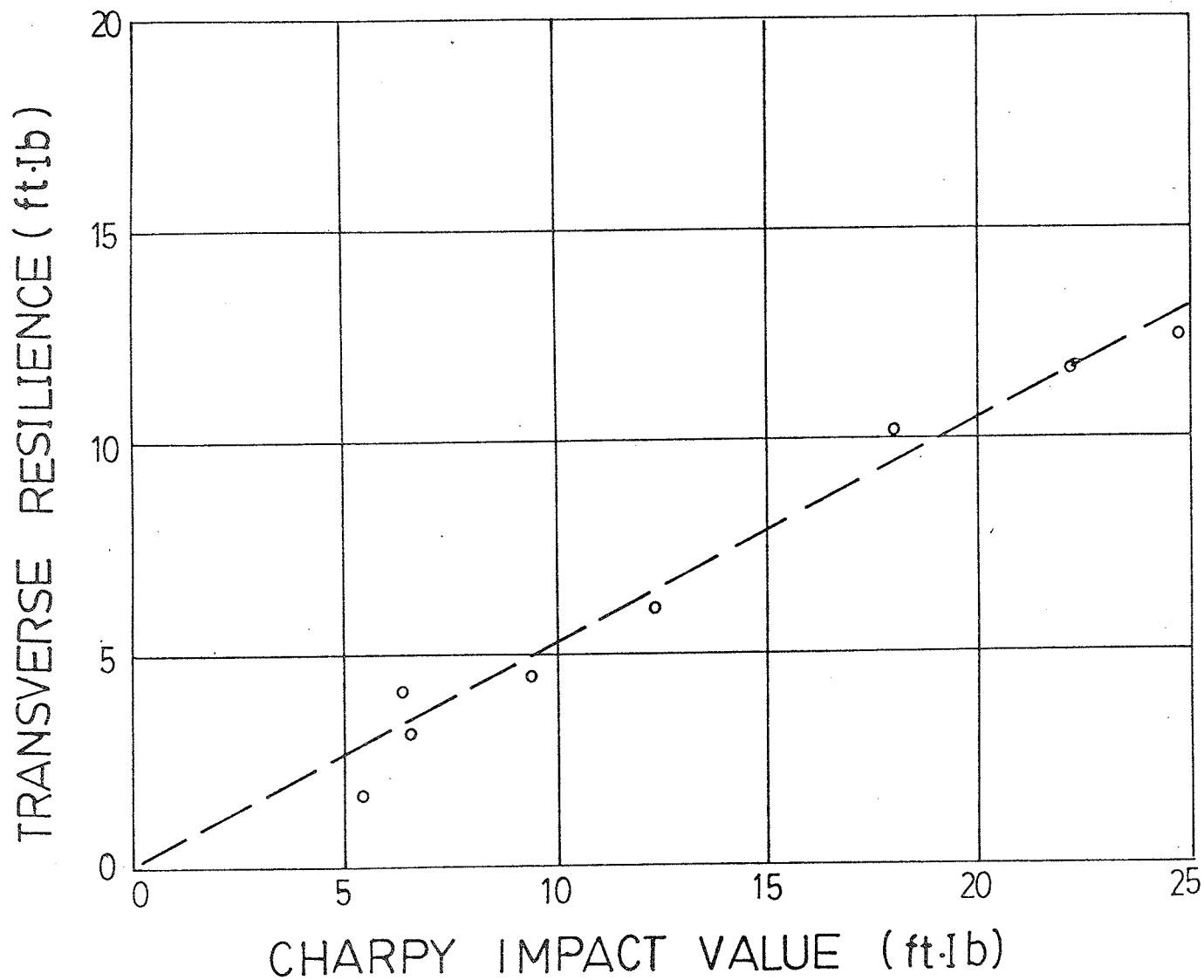


Fig. 8B The Relation Between Impact Strength of Gray Iron and Its Transverse Resilience^[5]

In gray cast iron material, a sharp notch reduces the energy to initiate a crack and as the energy to propagate the crack is low, the total energy absorbed will also be low. ASTM standard A327-72^[2] uses an unnotched cylindrical specimen in a Charpy-type impact test, because any notched specimen of gray cast iron would result in a decrease in the energy to failure and would make it more difficult to distinguish between the impact properties of the various gray cast irons.

Generally, the effect of section size from which the standard specimens are cut is less on impact strength than on tensile strength^[4].

An increase in temperature from 0° to 350°C reduces the impact strength of gray cast iron by about 10 percent. As the test temperature drops to -100°C, a 30 percent reduction of impact strength is obtained. Within the normal range of atmospheric temperatures, however, the temperature effect can be disregarded.

2.5 Proposed Instrumented Test for Impact Strength Measurement

From the review of the properties of gray cast iron, it has been shown that tensile and transverse strength are the most commonly used parameters in practice. Impact strength, though it is essential to the application under dynamic loading, is a relatively less understood parameter. All the impact tests determine the impact strength in terms of fracture energy. However, difficulties arise when correlation between energy values, as indicators of impact strength obtained from Charpy impact test, and the actual service conditions is required. It is desirable to know the failure stress of gray cast iron under impact loading. In the experimental study of this thesis, an effort is made to develop a series of instrumented impact tests, in order to investigate the failure stresses of gray cast iron under varying loading rates.

CHAPTER 3

EXPERIMENTAL STUDY

3.1 Introduction

The purpose of the experimental study was to investigate the effect of loading rate on the failure strength of gray cast iron. In particular,

(1) How does the failure strength of gray cast iron vary with varying loading rates?

(2) How is the failure strength of gray cast iron affected by the specimen shape and specimen size?

(3) Is there any difference in impact properties attributable to the change in the grade of gray cast iron?

To answer these questions, a series of static and impact tests on unnotched, U-notched and V-notched specimens was performed according to the test program shown in Table 4.

3.2 Material and Specimens

Two grades of gray cast iron, ASTM G20 and G40, were obtained from a local foundry as specimen material. The castings were cylindrical bars 16" in length and 1" in diameter. The chemical composition of the castings is given in Table 5.

Four types of specimen, all tensile, were machined from the as-cast bars. The dimensions of the specimen are given in Fig. 9.

LOADING SPECIMEN CONDITION CONFIGURATION	STATIC V = 0 ft/s	IMPACT VELOCITY V = 12 ft/s	IMPACT VELOCITY V = 16 ft/s	IMPACT VELOCITY V = 20 ft/s	IMPACT VELOCITY V = 24 ft/s
UNNOTCHED D = 0.5"					
U - NOTCHED D = 0.5"					
V - NOTCHED D = 0.5"					
UNNOTCHED D = 0.354"					

TABLE 4 TEST PROGRAM

G20 Gray Cast Iron

Carbon	3.59%
(Carbon Equivalent)	4.29%
Silicon	2.85%
Sulfur	0.05%
Phosphorus	0.01%
Manganese	0.5%

G40 Gray Cast Iron

Carbon	3.59%
(Carbon Equivalent)	4.29%
Silicon	2.10%
Nickel	1.5%
Manganese	0.5%
Sulfur	0.05%
Phosphorus	0.01%

Table 5 Chemical Composition of Test
Materials provided by the
Foundry.

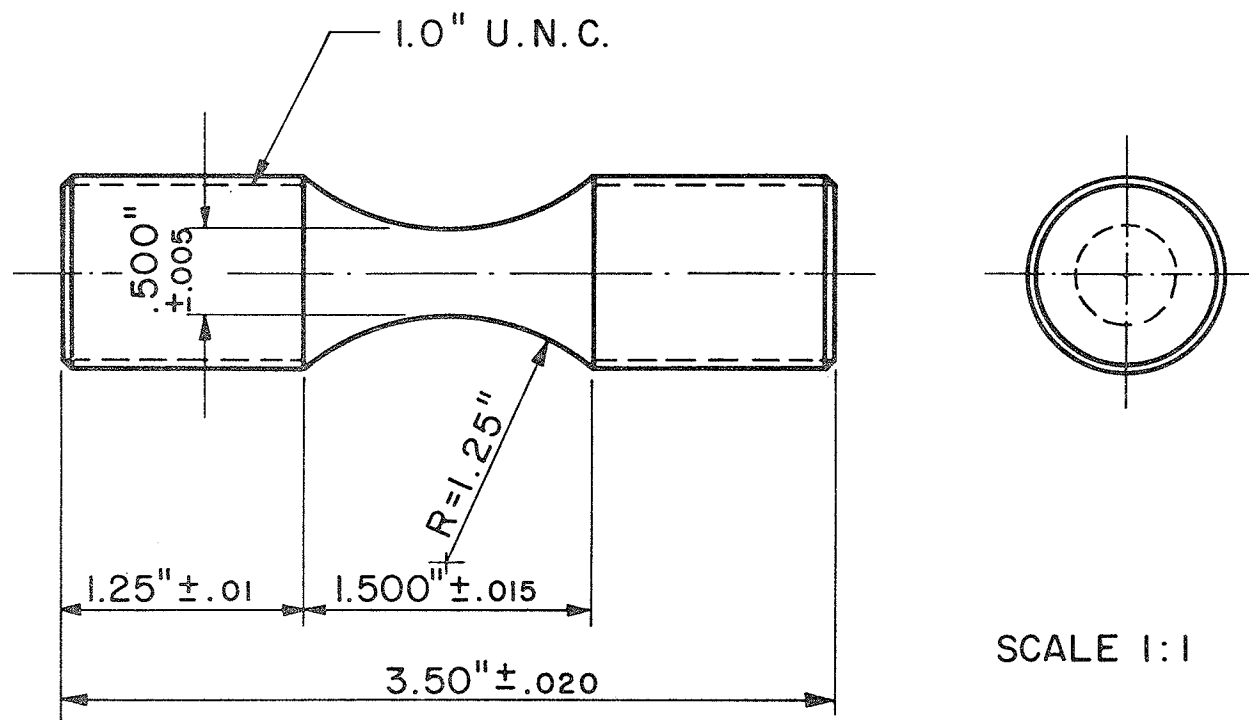


Fig. 9(A) Unnotched Tensile Specimen of Gray Cast Iron

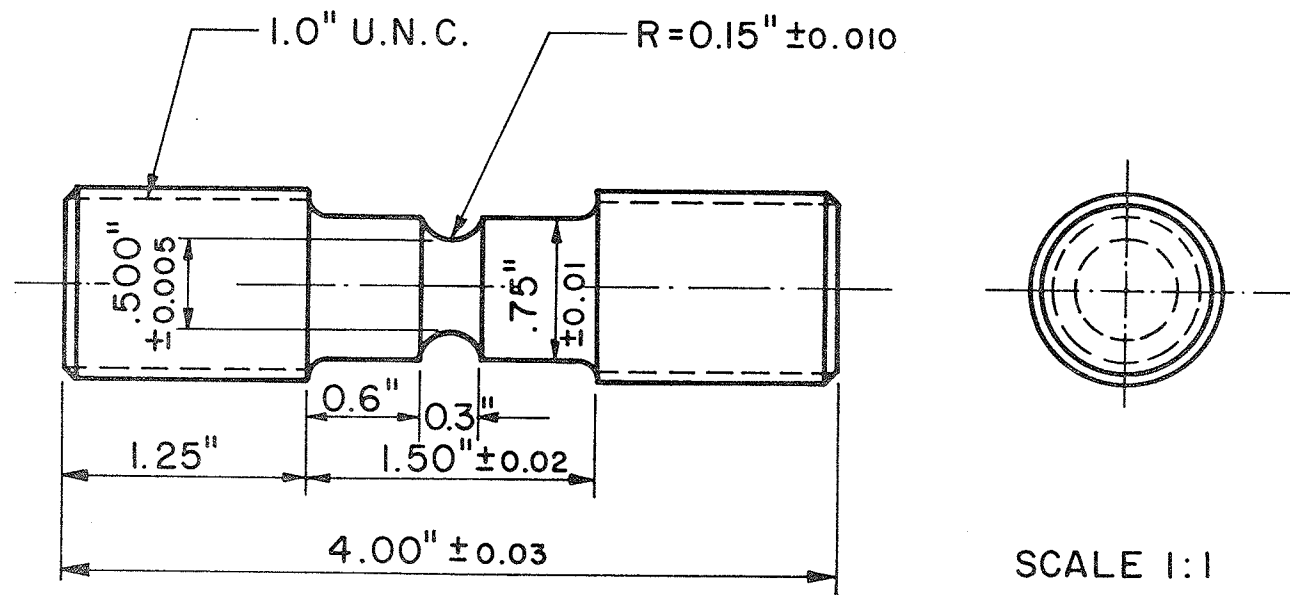


Fig. 9(B) U-notched Tensile Specimen of Gray Cast Iron

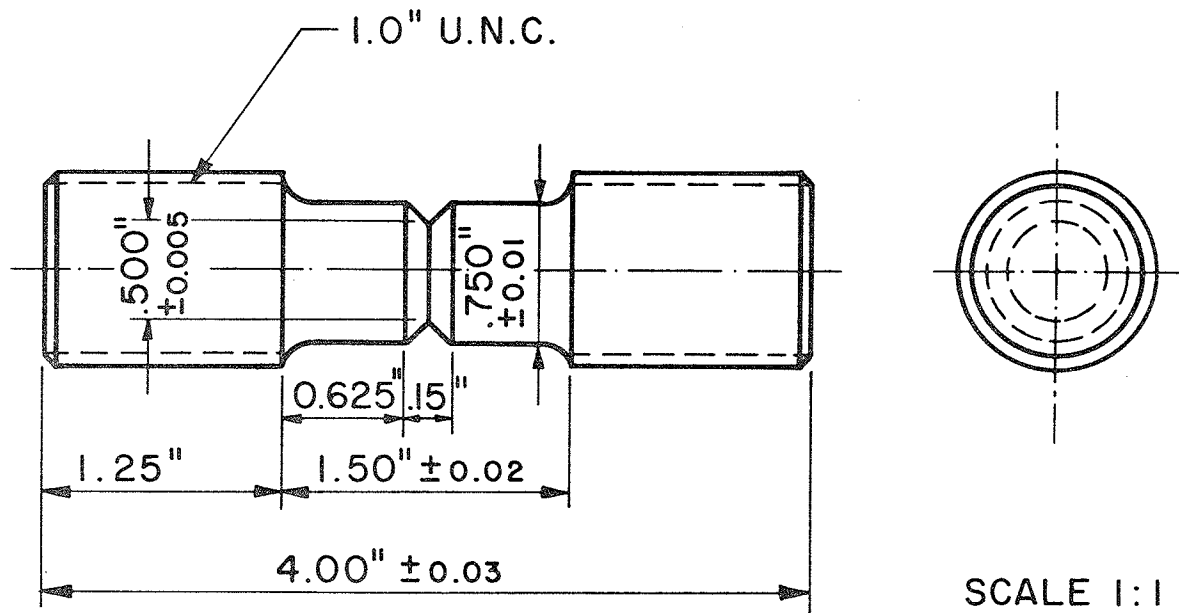
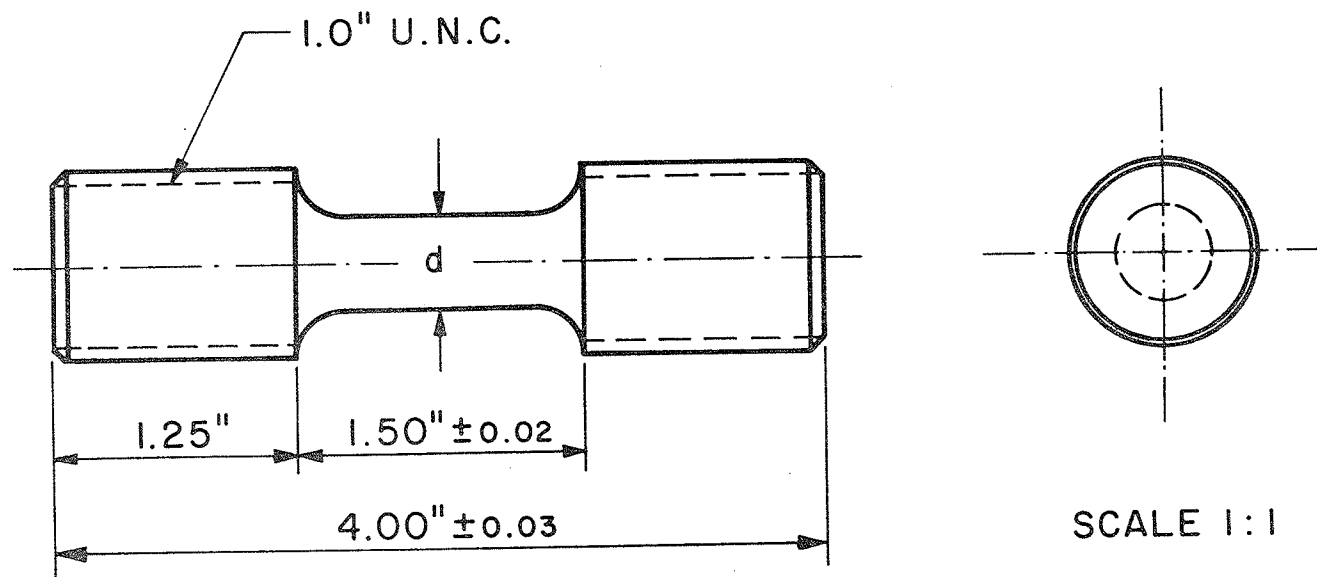


Fig. 9(C) V-notched Tensile Specimen of Gray Cast Iron



d (0.500 ± 0.005) (0.354 ± 0.005)

Fig. 9(D) Unnotched Tensile Specimen of Gray Cast Iron
with various Section Areas

3.3 Test Equipment

The static tensile tests were performed on a Gilmore Close loop testing machine and a Baldwin Universal testing machine.

The equipment used for the impact tensile test is shown schematically in Fig. 10. It consists of a drop weight testing machine, an anvil and load cell assembly, and electronic measurement instruments. The various components will now be described in some detail.

3.3.1 Drop Weight Testing Machine

The Drop Weight Testing Machine, as shown in Fig. 11, was designed and built for the impact tensile tests. It consists of a 50 pound drop weight guided by two cables of 0.3" in diameter. The test machine has a maximum drop height of ten feet, which could be equated to a total energy capacity of 500 foot pound with approximate maximum impact velocity of 25 feet per second. The testing machine includes an electric hoist for positioning the weight at any desired height and a mechanism for releasing it.

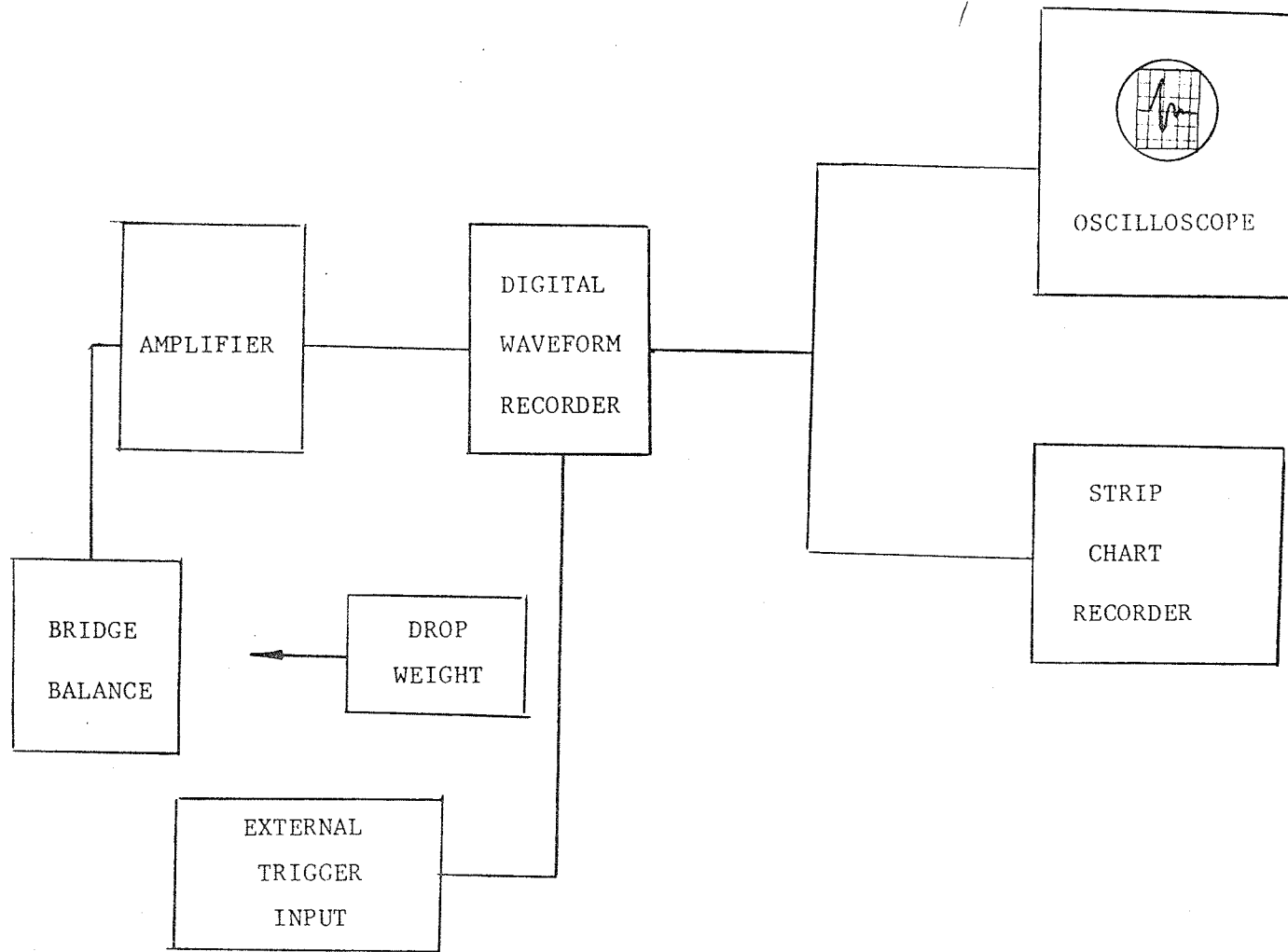


FIG. 10 SCHEMATIC DIAGRAM OF THE INSTRUMENTATION FOR THE INSTRUMENTED DROP WEIGHT TEST

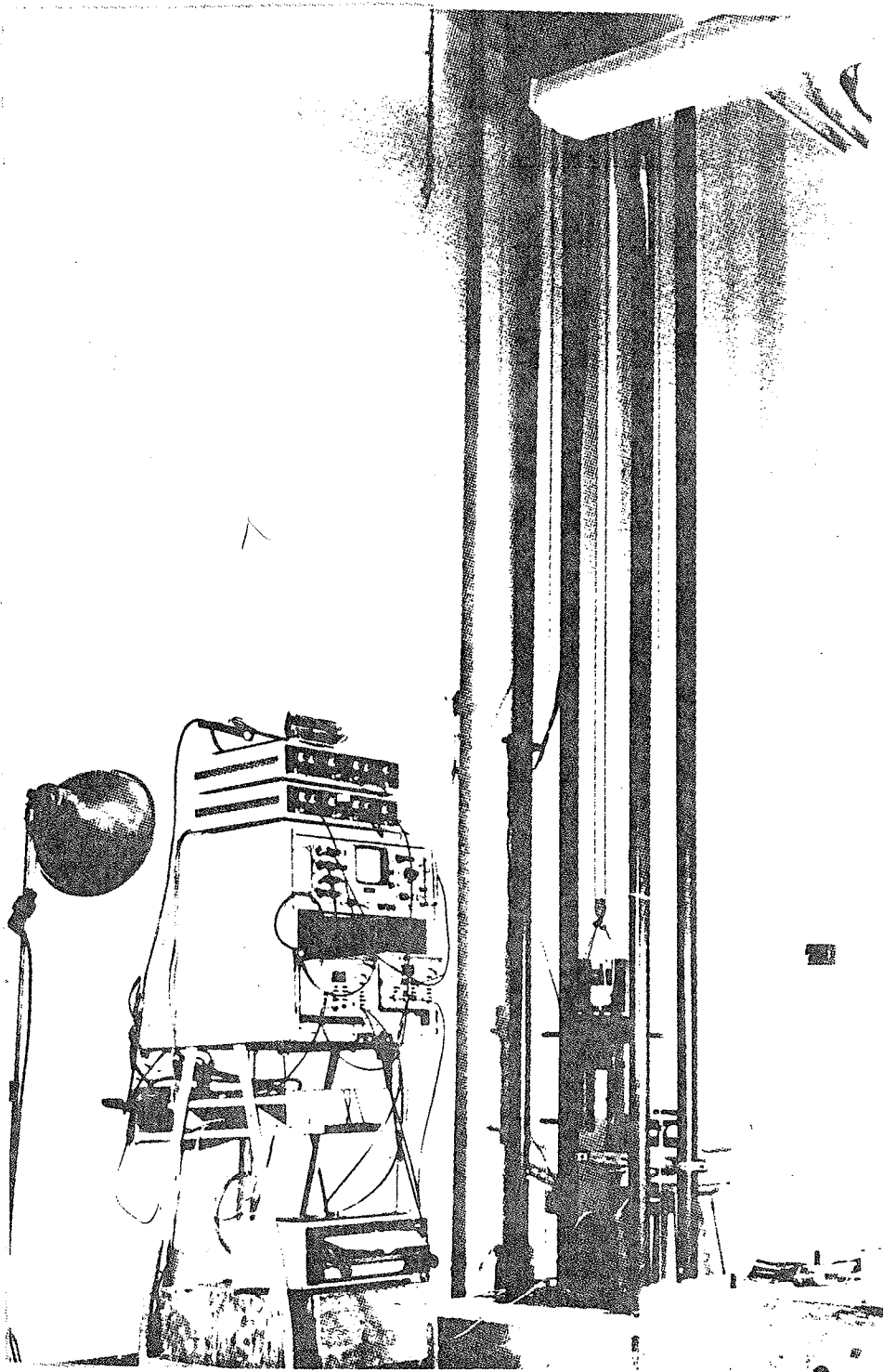


Fig.11 Drop Weight Testing Machine and Measurement Instrumentation

3.3.2 Load Cell and Anvil Assembly

The cylindrical specimen is held by two steel cross bars, as shown in Fig. 12. Electrical resistance strain gages on the upper cross bar make it a load cell or dynamometer. The Wheatstone bridge circuit, shown in Fig. 13, contains four active gages mounted on the upper crossbar. Excitation for the Wheatstone bridge circuit was supplied by 6V D.C. battery. The steel anvil assembly, shown in Fig. 14, consists of two parallel supporting bars mounted vertically on a 12" x 8" x 3/4" plate. It is fastened rigidly to the base of the drop weight testing machine. The upper crossbar, or the dynamometer, rests on the supporting bars of the anvil. The specimen and the lower crossbar are suspended between the supporting bars. The specimen is loaded in tensile impact when the drop weight strikes the lower crossbar.

3.3.3 Amplifier

A Rockland Model 432 IC operational amplifier, which provides highly stable gain and very low noise and distortion, was used in the impact tests. The nominal maximum gain of the amplifier is 100.

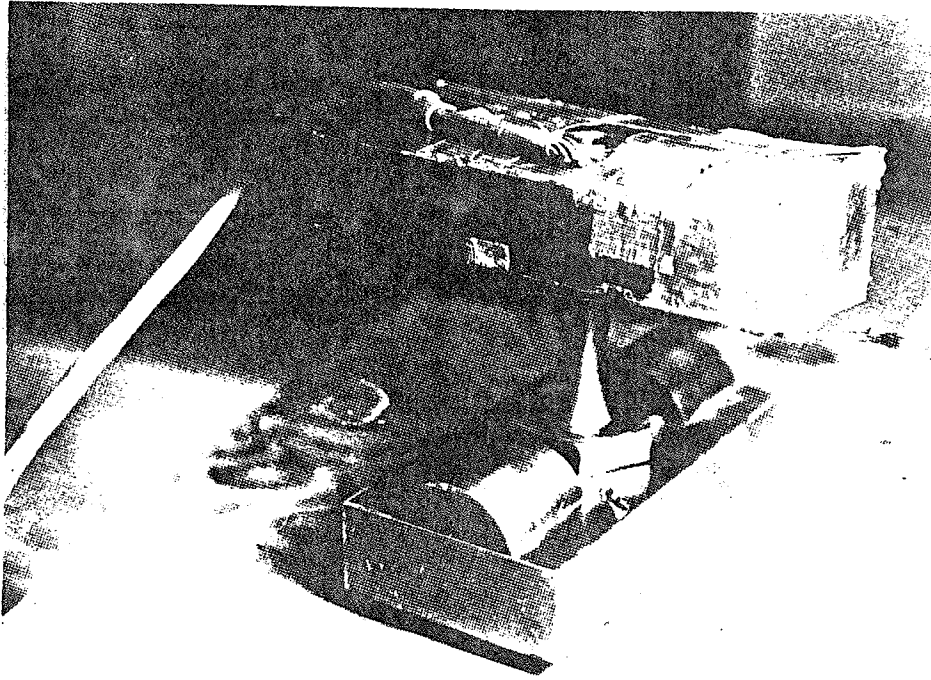


Fig. 12 Load Cell and Impact Specimen

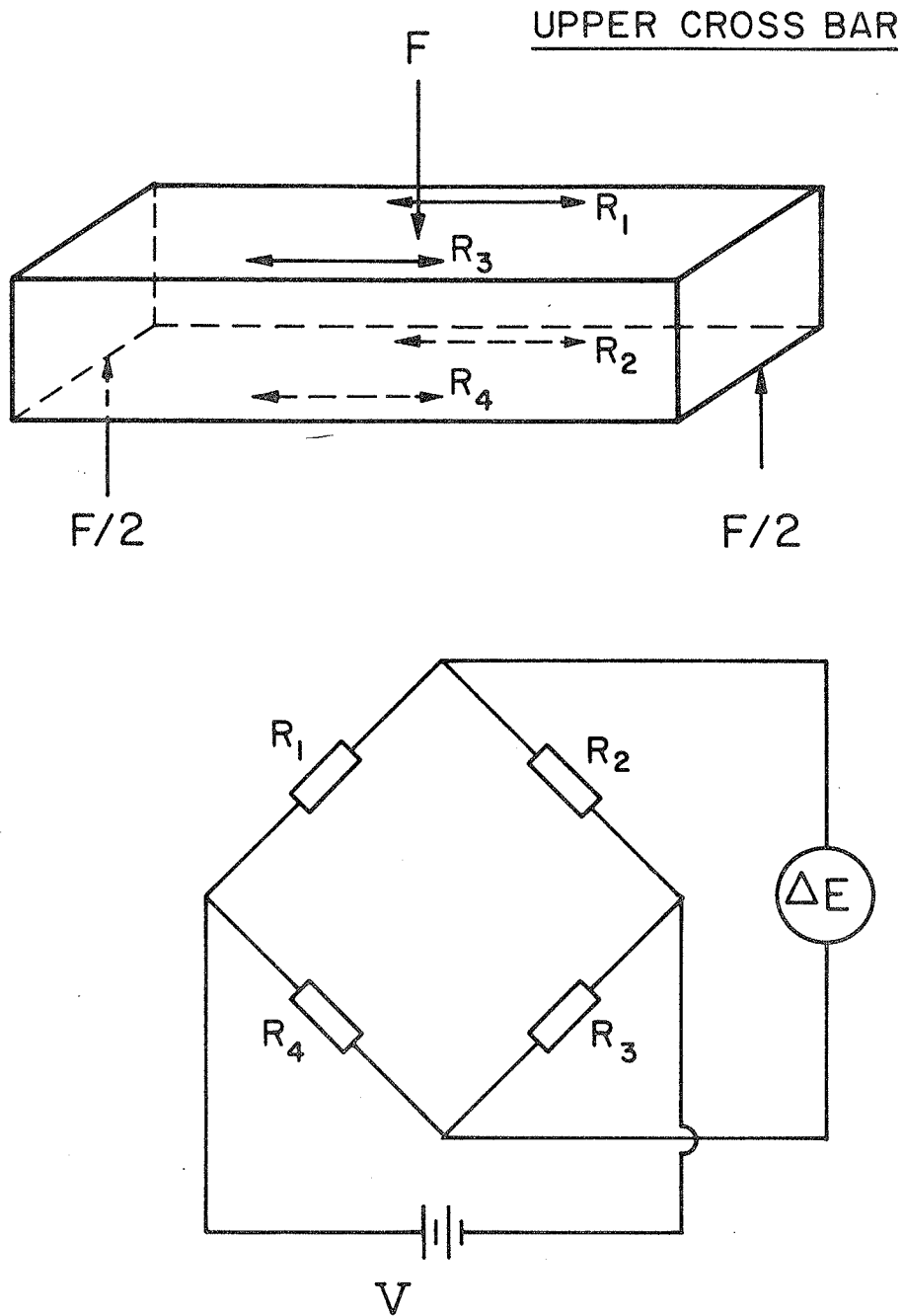
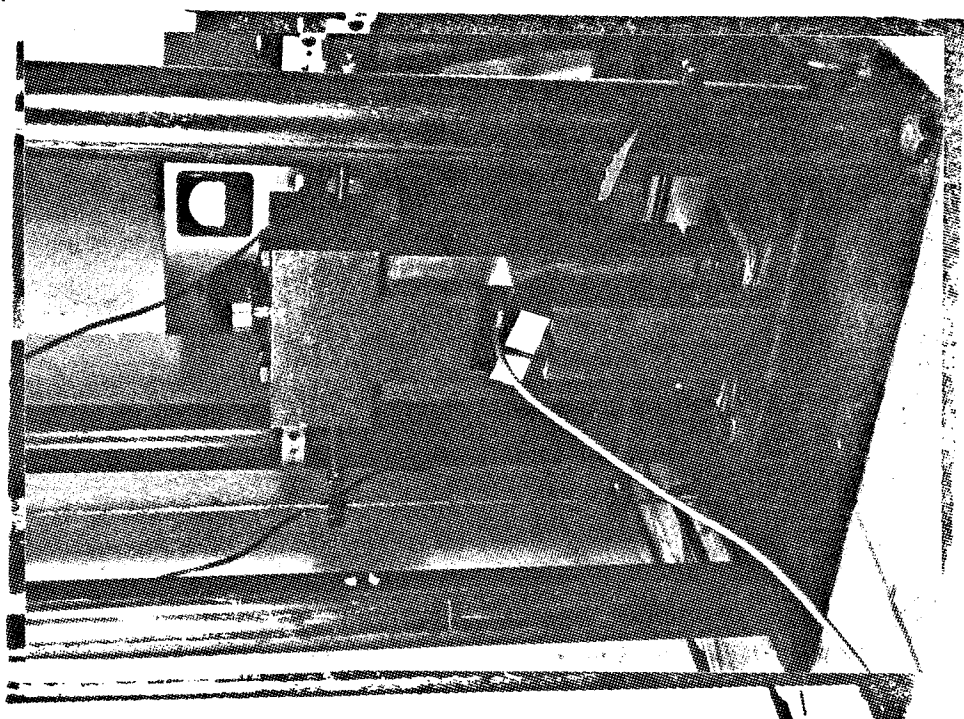
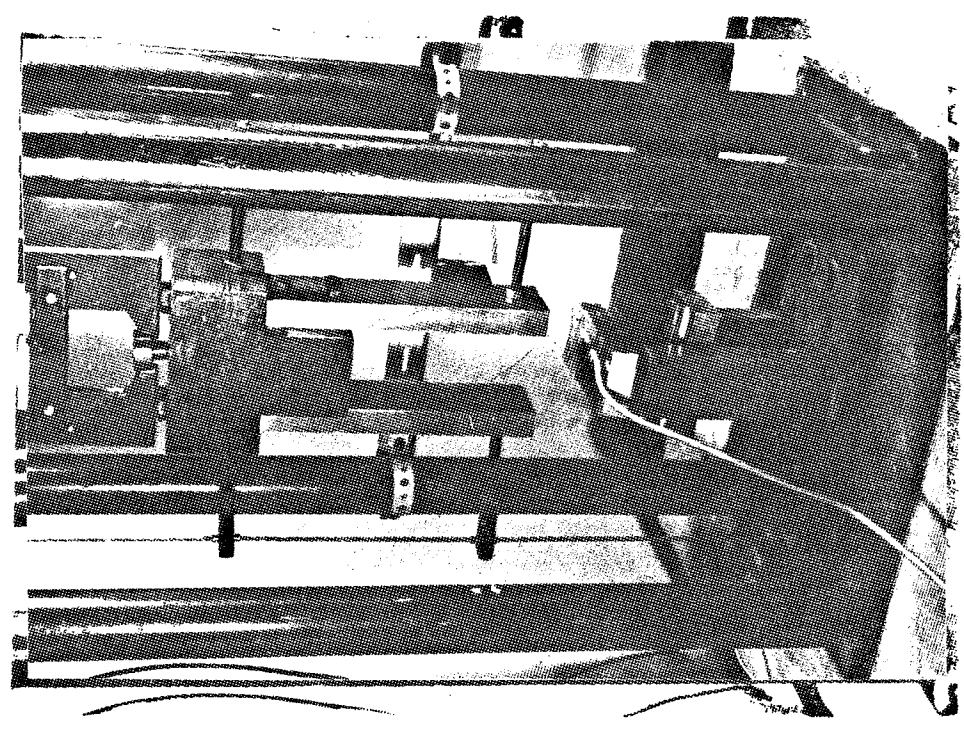


Fig.13 Schematic Diagram of Load Cell and Wheatstone Bridge Circuit



(a) Before



(b) After

Fig. 14 Anvil Assembly and Drop Weight

3.3.4 Waveform Recorder

The Waveform Recorder is a specific class of electronic instrument using digital techniques to record a preselected portion of an electric signal as it varies with time. Thus, the wave shape during the selected time period is recorded and held in the memory of the instrument.

A Biomatron, Model 805 waveform recorder was used in the impact tests. The output signal of the Wheatstone bridge circuit was first amplified and then fed into the waveform recorder. While the information was stored in the memory of the waveform recorder, it could be read out by connecting an oscilloscope or a strip chart recorder.

A maximum sampling rate of 200 KHz (minimum interval of 5 μ sec) was used during the impact tests. 2048 samples were taken on each record.

The trigger of the waveform recorder was supplied from an external D.C. current, controlled by a micro-switch placed in the path of the falling weight.

3.3.5 Strip Chart Recorder

A Plikadeni Model B-107 strip chart recorder was used to obtain the final load-time record from the memory of the waveform recorder. Various chart speeds could be used, ranging from 5 cm per min. to 60 cm per min.

3.4 Calibration of the Test Equipment

The calibration procedure is discussed in detail in Appendix A.

The instrumented upper cross bar, used as a load cell, was calibrated. The electronic measurement system, including the amplifier, the waveform recorder, and the strip chart recorder was also calibrated to ensure the accurate recording and measurement of the strain signal during the impact tests.

3.5 Test Procedure

The test program indicated in Table 5 was followed.

3.5.1 Static Tensile Test

Unnotched, U-notched and V-notched specimens of both G20 and G40 were tested. As noted previously, the tests were performed on the Gilmore Closed-Loop testing machine and the Baldwin Universal testing machine.

3.5.2 Impact Tensile Tests

The following procedure was used in all the tensile impact tests.

The cylindrical specimen was screwed into the two cross bars. Two nuts were used to lock the ends of the specimen to the cross bars, as previously shown in Fig. 12. The specimen and the cross bars were positioned

on the anvil. A few layers of lead strip were placed between the two supporting bars at the bottom of the anvil in order to absorb the shock from the drop weight and lower cross bar after impact fracture. The drop weight was raised to the desired drop height.

In preparation for the actual loading, the excitation voltage of the Wheatstone Bridge circuit was checked and recorded.

Finally, the drop weight was released. It fell and broke the specimen.

The force-time relation was automatically recorded by the waveform recorder during the impact test. The oscilloscope and strip chart recorder which were connected to the waveform recorder gave the final results to be visualized and analysed.

CHAPTER 4

TEST RESULTS

4.1 Results of the Static Tensile Tests

The results of the static tensile tests on the specimens with various grades, configurations and sizes are summarized in Table 6 and Table 7.

The data of the failure forces were obtained from the force-elongation records of the tests. The failure stresses were the failure forces divided by the original cross sectional areas of the specimens.

4.2 Results of the Impact Tensile Tests

The results of the impact tensile tests were obtained from the outputs of the oscilloscope and the strip chart recorder. In contrast with force-elongation information in the static tensile tests, force-time information was provided during the impact tests.

4.2.1. Force-Time Record

Typical force-time records are shown in Fig. 15, 16 and 17. In these records, the most significant parameters are the peak force value F_p and the loading time T_L . The loading time T_L is defined as the time required to load the load cell from zero to peak force value.

The interpretation of the force-time record is discussed in detail in Chapter 5.

	No	Diameter (in)	Failure Force (lb)	Failure Stress (PSI)	Mean Stress (PSI)
Unnotched (Zero Gage Length)	1	0.493	4750	24,896	
	2	0.498	4600	24,097	24,462
	3	0.490	4600	24,393	
U-notched	1	0.5	4300	21,900	21,750
	2	0.498	4230	21,600	
V-notched	1	0.5	3800	19,387	19,770
	2	0.5	3950	20,153	

Table 6
Static Test Results of G20 Specimens



	No	Diameter (in)	Failure Force (lb)	Failure Stress (PSI)	Mean Stress (PSI)
Unnotched (Zero Gage Length)	1	0.496	7070	36,071	
	2	0.490	5950	30,357	33,785
	3	0.496	6650	33,928	
U-notched	1	0.5	6000	30,612	30,101
	2	0.5	5800	29,591	
V-notched	1	0.5	5450	27,800	27,800
Unnotched (Gage Length L = 2")	1*	0.503	4600	23,440	27,006
	2	0.5	6000	30,573	
	3	0.354	2900	29,480	29,988
	4	0.354	3000	30,496	

* A large flaw was found in the fracture surface of this specimen.

Table 7
Static Test Results of G40 Specimens

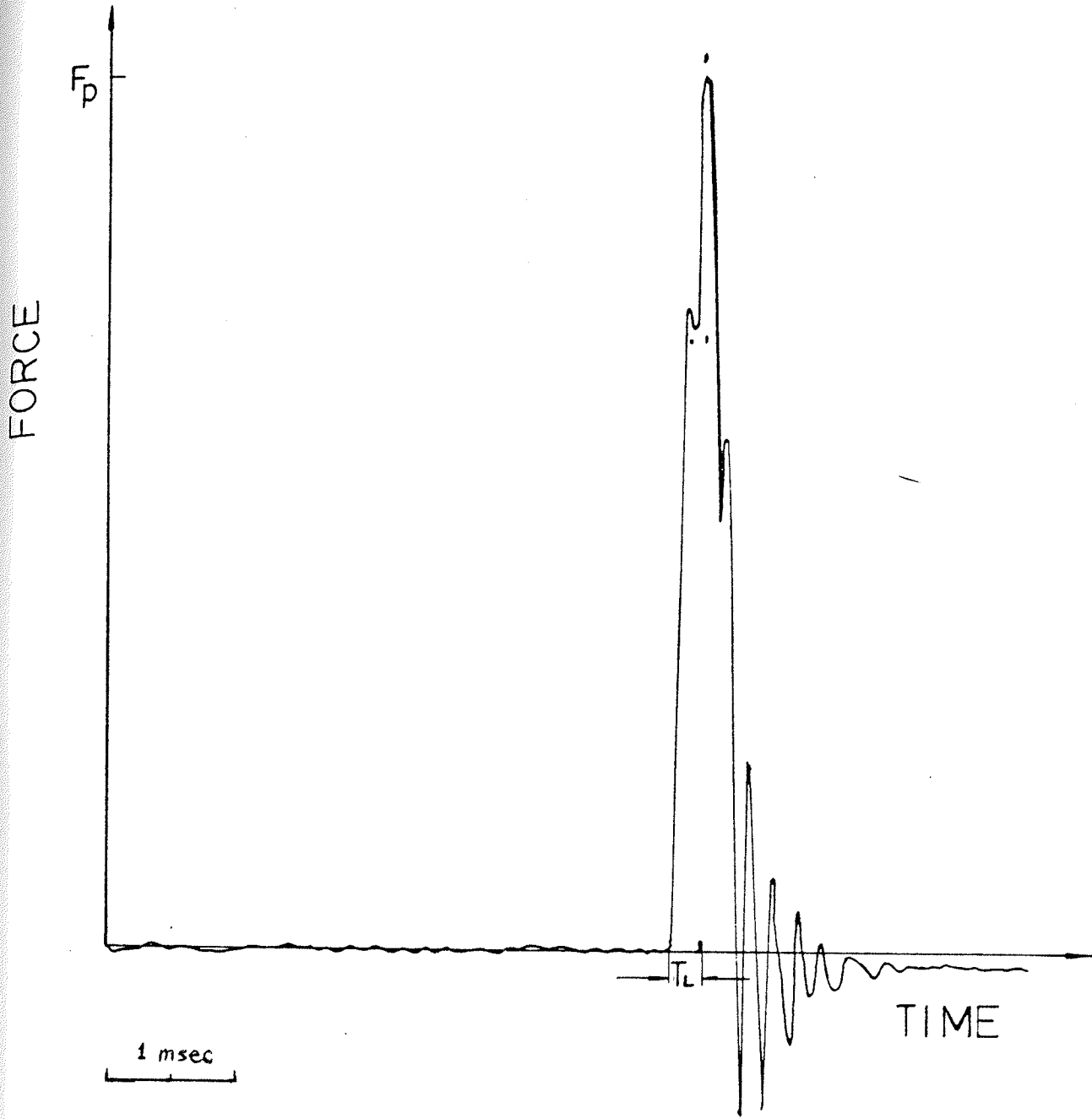


Fig. 15 Typical Force-time Record from Strip Chart Recorder (Impact Velocity 12 ft/sec)

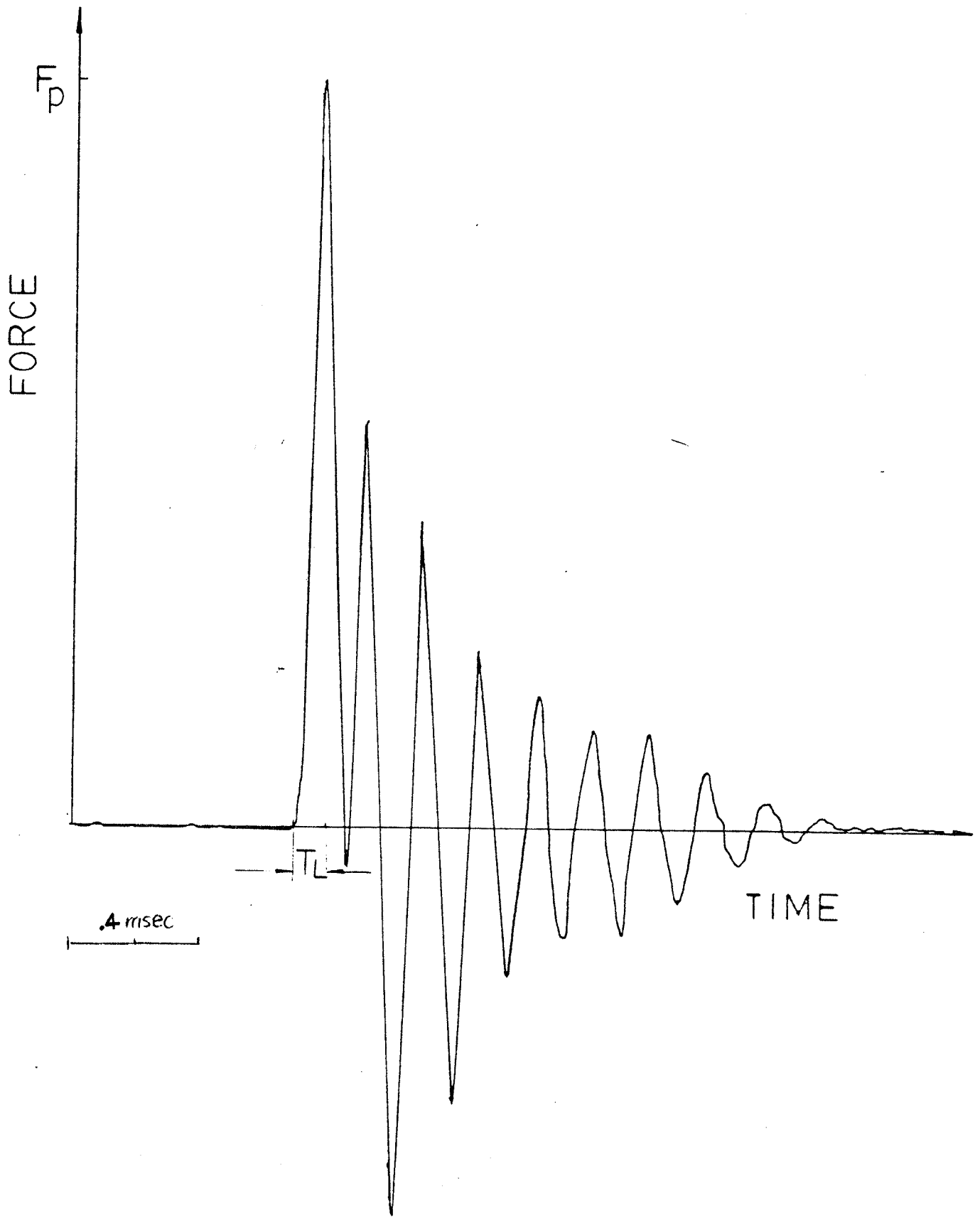


Fig. 16 Typical Force-Time Record from Strip Chart Recorder (Impact Velocity 24 ft/sec)

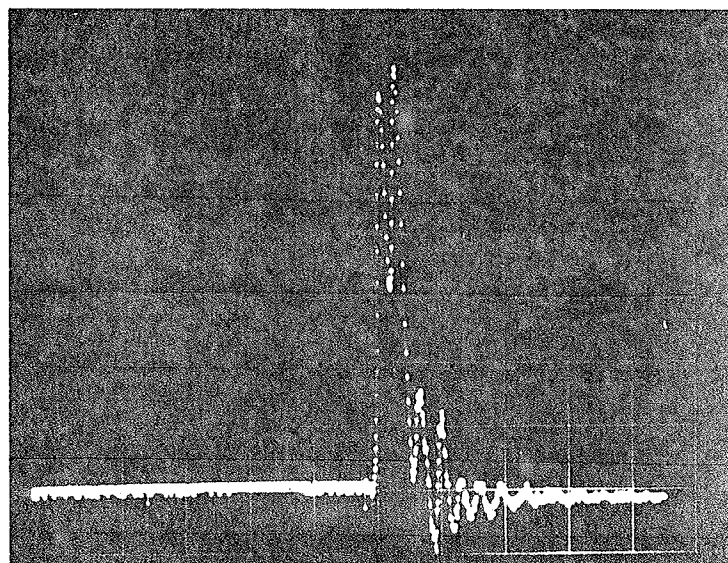
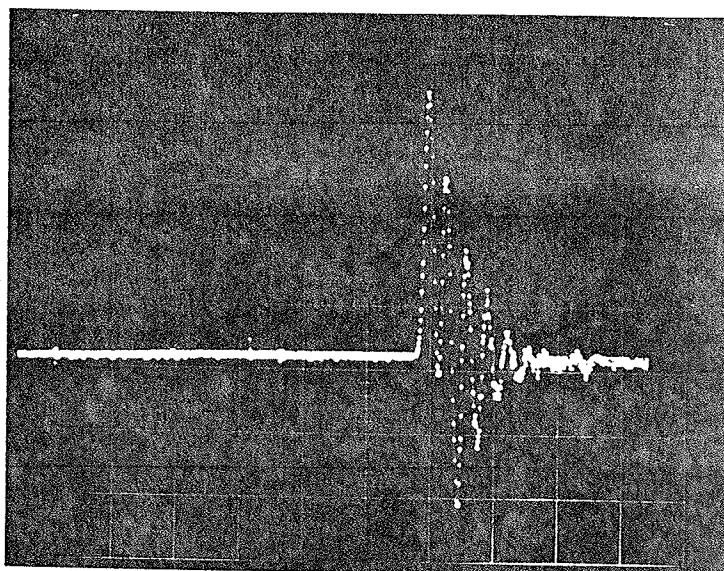


Fig. 17 Typical Force-Time Records from Oscilloscope

4.2.2. Impact Test Results of G20 Specimens

G20 cylindrical specimens - unnotched, U-notched and V-notched - were tested to failure under various impact velocities, ranging from 12 ft/sec. to 24 ft/sec. The test results are summarized in Table 8 and Table 9.

The stress terms in Table 9 and Table 10 were calculated by dividing the peak force value F_p by the cross sectional area of the specimen. this value should not be simply considered as the failure stress of the specimen without further analysis.

4.2.3. Impact Test Results of G40 Specimens

Following the same format as that for G20 specimens, the test results for the G40 specimens with different configurations and sizes are summarized in Table 10 and Table 11. In addition, the impact test results of the unnotched specimens with gage length $L = 2"$ and different diameters are shown in Table 10.

Impact Velocity V (Ft/sec)	No	Loading Time T_L (M sec)	Peak Force Value F_p (lb.f)	Stress σ^* (KSI)	Mean σ^* (KSI)
Unnotched Specimens with zero gage length (D = 0.5")	1	0.288	6523	32.84	34.563
	12	2	0.280	7076	
	3	0.280	6879	34.50	
16	1	0.24	8147.2	40.696	42.233
	2	0.23	8901.9	43.77	
20	1	0.13	7200	36.69	35.925
	2	0.15	6899	35.16	
24	1	0.096	7223	36.852	37.756
	2	0.096	7578	38.66	

σ^* - Nominal stress, calculated by dividing F_p by the cross sectional area of the specimen.

Table 8 Impact Test Results of the Unnotched G20 Specimen

	Impact Velocity V (Ft/sec)	No	Loading Time T_L (M sec)	Peak Force Value F_p (lb.f)	Stress σ^* (KSI)	Mean σ^* (KSI)
U-Notched		1	0.28	5292	26.966	
Specimens	12					26.418
(D = 0.5")		2	0.28	5077	25.878	
		1	0.240	6468.2	32.96	
	16	2	0.240	6058.5	30.872	31.916
V-Notched		1	0.27	5428.3	27.66	
Specimens	12					27.48
(D = 0.5")		2	0.28	5355.8	27.30	
		1	0.240	6218.6	31.692	
	16	2	0.238	5597.5	28.50	30.493
		3	0.230	6140.0	31.29	

σ^* - Nominal stress, calculated by dividing F_p by the cross sectional area of the specimen.

Table 9 Impact Test Results of the Notched G20 Specimen

Impact Velocity V (Ft/sec)	No	Loading Time T_L (M sec)	Peak Force Value F_p (Ib.f)	Stress σ^* (KSI)	Mean σ^* (KSI)
U-Notched	1	0.28	6843.9	34.92	
Specimens (D = 0.5")	12				34.7
Zero Gage	2	0.27	6778.3	34.583	
Length	1	0.24	7462	38.07	
	2	0.24	7512	38.33	38.20
	24	0.1	5350.3	27.3	27.3
Unnotched (D = 0.5")	1	-	5900	30.05	
Gage length (L = 2")	2	-	6578	33.6	31.80
Unnotched (D = 0.354")	1	-	3382.3	34.387	
Gage Length (L = 2")	2	-	3669.4	37.3	35.80

σ^* - Nominal stress, calculated by dividing F_p by the cross sectional area of the specimen.

Table 10 Impact Test Results of the Unnotched G40 Specimen

Impact Velocity V (Ft/sec)	No	Loading Time T_L (M sec)	Peak Force Value F_p (lb.f)	Stress σ^* (KSI)	Mean σ^* (KSI)	
U-Notched	1	0.28	7254.2	37.016		
Specimens (D = 0.5")	12				36.19	
	2	0.28	6931.7	35.37		
	16	1	0.23	7089.2	36.17	36.17
V-Notched	1	0.28	6522.1	33.28		
Specimens (D = 0.5")	12				32.92	
	2	0.28	6380.3	32.55		
	16	1	0.24	6636.7	33.862	33.86

σ^* - Nominal stress, calculated by dividing F_p by the cross sectional area of the specimen.

Table 11 Impact Test Results of the Notched G40 Specimens

CHAPTER 5

DISCUSSION AND ANALYSIS

5.1. INTRODUCTION

The procedure to analyze results of static tensile tests is quite standardized. However, in analysis of the impact test results, the question of the system response arises. This question relates to the validity of the test results and must be resolved properly.

In this chapter, the static test results will be discussed first.

A method employed to interpret the impact test results with consideration of the system response is described. According to the analysis of the system response and the test results, the loading rate effect to the failure strength of gray cast iron will be discussed.

5.2 Discussion of the Static Test Results

In the static tensile tests, it was found that the G40 castings, as received from the foundry, did not meet the ASTM A48 standard. The average tensile strength of the G40 specimens was 34 KSI. Since the purpose of the experimental study was to investigate the loading rate effect on failure strength of gray cast iron, it was sufficient that the castings provided a different grade of cast iron for comparison with the G20 castings.

For both G20 and G40 specimens, the failure stresses of the notched specimens were found to be 10 - 15 % less than that of the unnotched ones. The difference of the failure stress between U-notched and V-notched specimens was within 8%.

No significant size effect was found from the results of the static tests.

5.3 Dynamic Response of the System to Impact Loading

It is known that statically, the load applied to the specimen is directly proportional to the deflection of the load-cell. However, during impact loading because of the mass involved, the system (cross bars-specimen) experiences a vibration which is superimposed on the main tensile fracture pulse. The deflection of the load-cell is not a simple function of the applied load. In order to calculate the real fracture force of the specimen from the output signal of the load cell, an analytical method is used and described as follows.

A simplified model of the test system is shown in Fig. 18. K_e , M_e and C_e are equivalent stiffness constant, mass and damping coefficient respectively. The anvil which supports the cross bars-specimen system is assumed rigid. $F (+)$ is the input forcing function which is assumed as a ramp force impulse in the impact tensile tests.

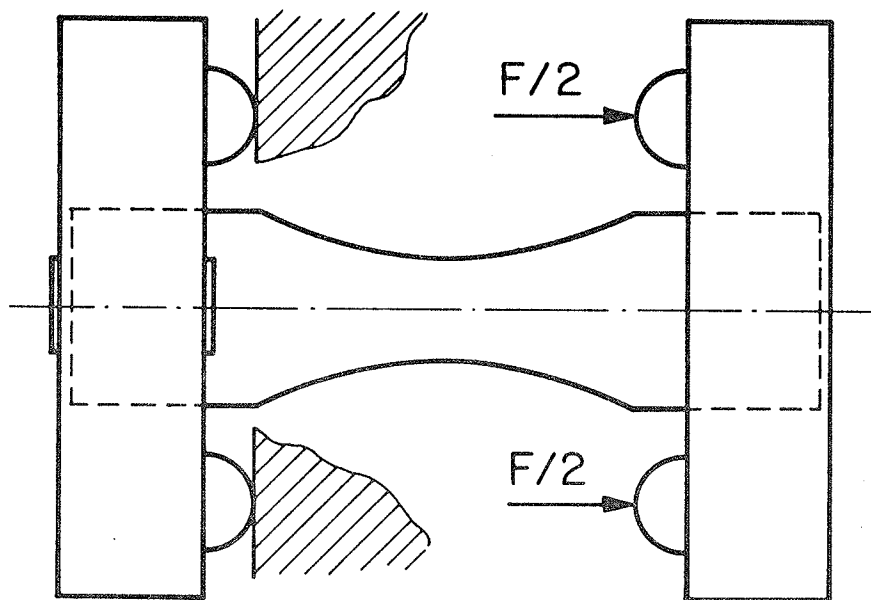
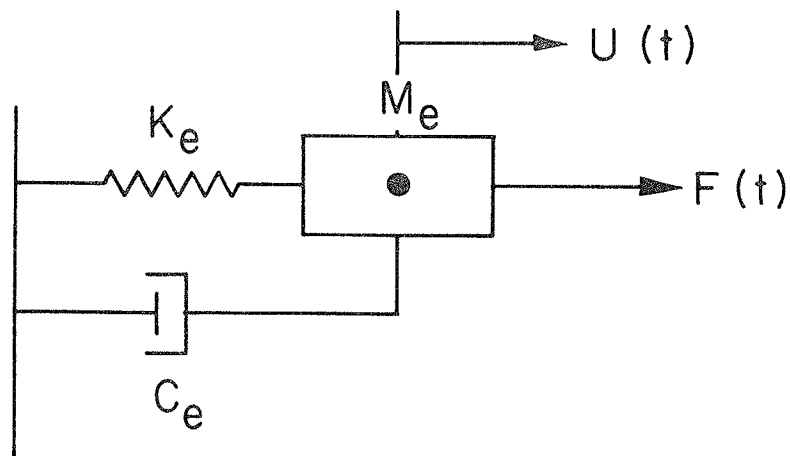


Fig. 18 Schematic Diagram of the Equivalent Cross Bars - Specimen System

The motion of the system could be described as:

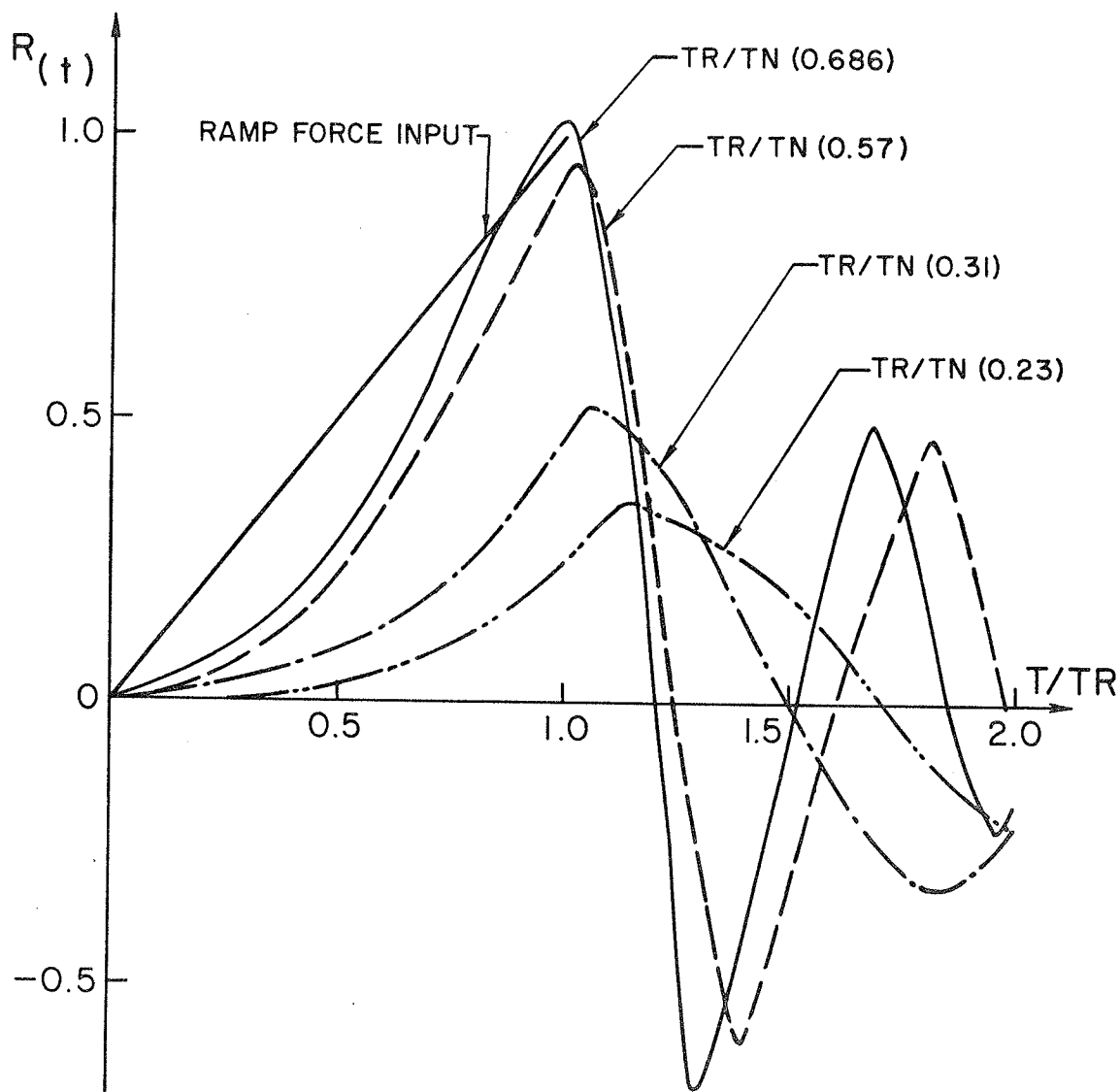
$$M_e \ddot{U} + C_e \dot{U} + K_e U = F(t)$$

The analytical solution of this equation is given in Appendix B. A plot of the solution in terms of response ratio versus time ratio is shown in Fig. 19. The four curves in Fig. 19 represent the solutions of the equation corresponding to four different time ratios TR/TN . The term TR in Fig. 19 is the rise time of the ramp impulse, and TN is the natural period of the vibration system which is the cross bars-specimen system in the experiment. $R(+)$ is the response ratio, or dynamic load factor, defined by:

$$R_{(+)} = \frac{\text{dynamic response (output of load cell)}}{\text{static deflection (real force input,)}}$$

The overshoot or undershoot values of R_{\max} are measures of discrepancy which arise from using the dynamic response to represent the ramp force impulse.

Since the time shift between the maximum values of the ramp force impulse and the system response output is very small (usually less than 10 μsec), the rise time of the ramp force impulse is considered roughly the same as the loading time TL , which could be measured from the force-time records of the impact tests.



RESPONSE RATIO TR/TN	0.686	0.57	0.31	0.23
IMPACT VELOCITY, FT/SEC	12	16	20	24

Fig. 19 Response of SDOF System to Ramp Impulse
(with Damping Coefficient $\xi = 0.15$)

The damping of the system contributes very little to the peak value of the system response. The R_{\max} value decreases approximately 1% as the damping coefficient increases from 0 to 0.5. In analysis of the R_{\max} values, the error caused by damping can be ignored.

In order to assure the validity of the impact test results, the natural frequency of the cross bars-specimen system must be known. This was determined by impulse testing in conjunction with a Digital Fourier Analyzer. The fundamental frequencies of the system were found to be 2.4 KHZ and 5.6 KHZ before and after the breakage of the specimen respectively. The corresponding natural periods were 0.42 msec and 0.18 msec respectively.

5.4 The Frequency Response of the Load Cell

In addition to the system response to dynamic loading, the frequency response of the load cell was checked to ensure that there would not be any significant distortion of the outputs from the load cell. In the drop weight tests, the time interval required for the travel of an elastic longitudinal wave between lower and upper cross bar was calculated to be 10 μ sec, and the transit time interval of the elastic stress wave reaching and passing over the strain gage length was 1.5 μ sec. Both of those time intervals are much shorter than the shortest loading

time which was approximately 100 μ sec. Since the distortion due to the frequency response of the load cell depends on the ratio of the travel time interval to the rise time of the stress wave, and as the value of this ratio was less than 10% in the experiment, the distortion caused by the response delay of the load cell can be neglected.

5.5 Discussion of the Impact Test Results

From the impact test results of both the G20 and G40 specimens presented in Chapter 4, it can be seen that the peak force value of the force-time records increases as the impact velocity increases from 12 ft/sec to 16 ft/sec, and then drops as the impact velocity increases further to 24 ft/sec.

The loading time TL is found to be approximately proportional to the impact velocity regardless of the shape and grade of the specimen. The relationship between impact velocity and loading time TL is plotted in Fig. 20.

Based on the data of natural period TN and the loading time TR (TL) measured from the impact tests, four characteristic response curves, corresponding to the impact tests with four impact velocities, were constructed, as previously shown in Fig. 19.

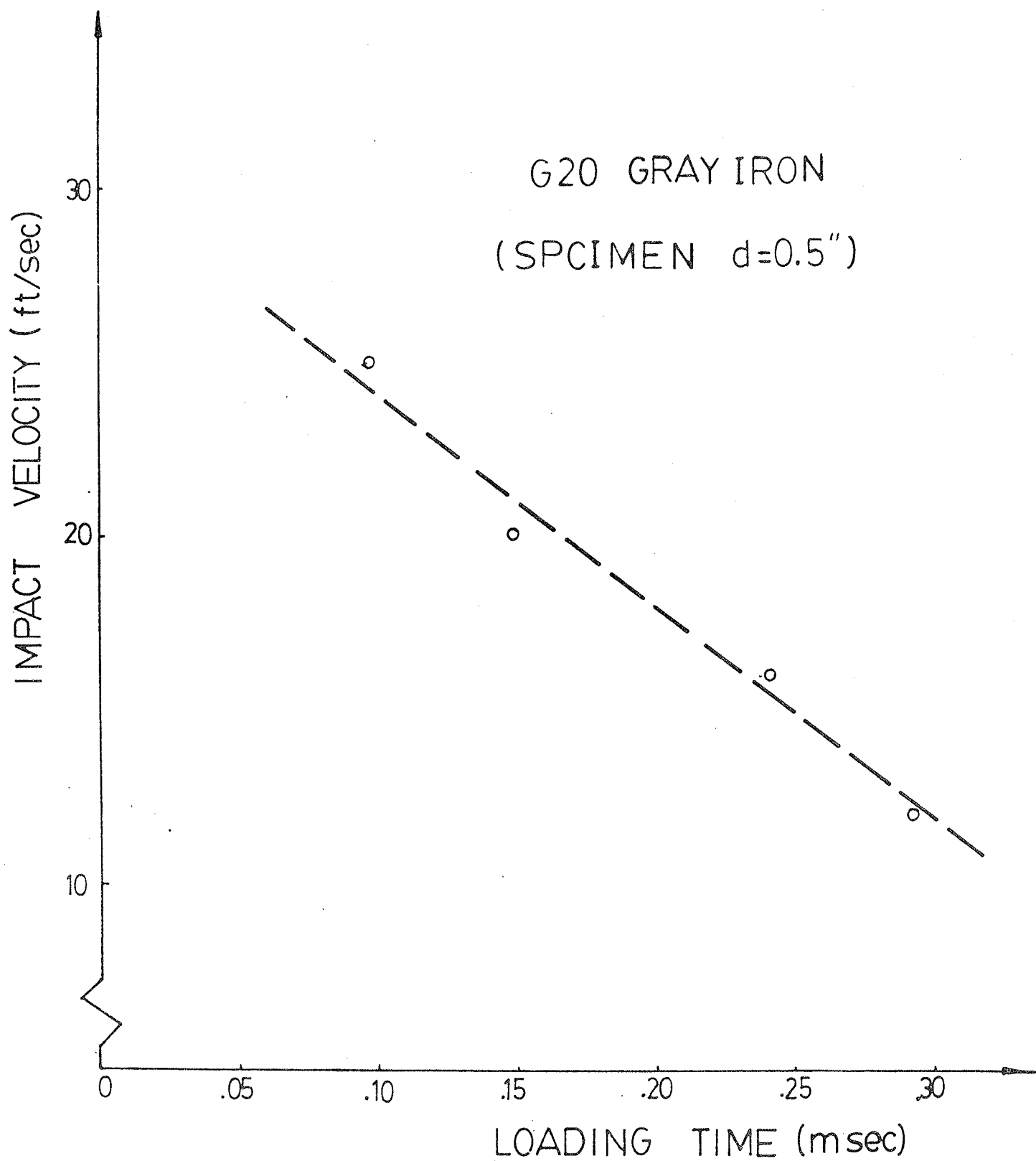


Fig. 20 The Relation Between Impact Velocity and Loading Time

From Fig. 19, it can be seen that as the impact velocity increases, the ratio of TR/TN decreases, and the R_{\max} value decreases. The R_{\max} values of the impact tests with impact velocity of 12 ft/sec and 16 ft/sec are 1.02 and 0.95. This indicates that the use of load cell output to represent the applied force may have 5% error, which is considered acceptable in most dynamic testing cases. However, the R_{\max} values of the tests with impact velocities of 20 ft/sec and 24 ft/sec were only 0.517 and 0.35, which implies that the output peak force values from the load cell were 51.7% and 35% of the input forces. Since the test system failed to respond to the input force faithfully, the peak force values of the impact tests with impact velocities of 20 ft/sec and 24 ft/sec are not considered as real fracture forces. One possible way to correct this output force is to use the response ratio or dynamic load factor, as described previously. A real fracture load may be obtained by dividing the peak force value of the test by the corresponding response ratio. If the peak force value of the force-time record is 100 lbf and the corresponding response ratio of the impact test is 0.5, then the real fracture force may be considered 200 lbf. However, since the analysis of the system was based on a model with simplified assumptions, the calculated ratio R_{\max} should be applied with some caution. The higher the impact velocity, the more significant is error caused by this method.

Fig. 21 and Fig. 22 show the loading rate effect to the failure stress of the G20 and G40 specimens. The solid lines in the figures show the experimental results directly from Tables 9 to 12. The dotted line in Fig. 21 shows the corrected values. It can be seen that the failure stress in both G20 and G40 specimens with unnotched, U-notched and V-notched configurations increases as the loading rate increases. The failure stress of the G20 specimens increases 50% - 60% as the impact velocity varies from zero (static loading) to 16 ft/sec. The tests of the G40 specimens show a 20% increase within the same range of the loading rates. These tests results indicate that the tensile strength of gray cast iron clearly exhibits loading rate dependence.

In the static tensile tests the gray cast iron specimens had an elongation at failure of less than 1%. All the specimens, statically and dynamically tested failed without any general plastic deformation. This is mainly due to the fact that the graphite in the castings is present in flake form. Each graphite flake is a stress raiser, and the stress concentrations occur at the boundaries of the flakes causing local plastic deformation. The plastic zones around the boundaries of the flakes are confined by material which was only elastically deformed. As the applied load continuously

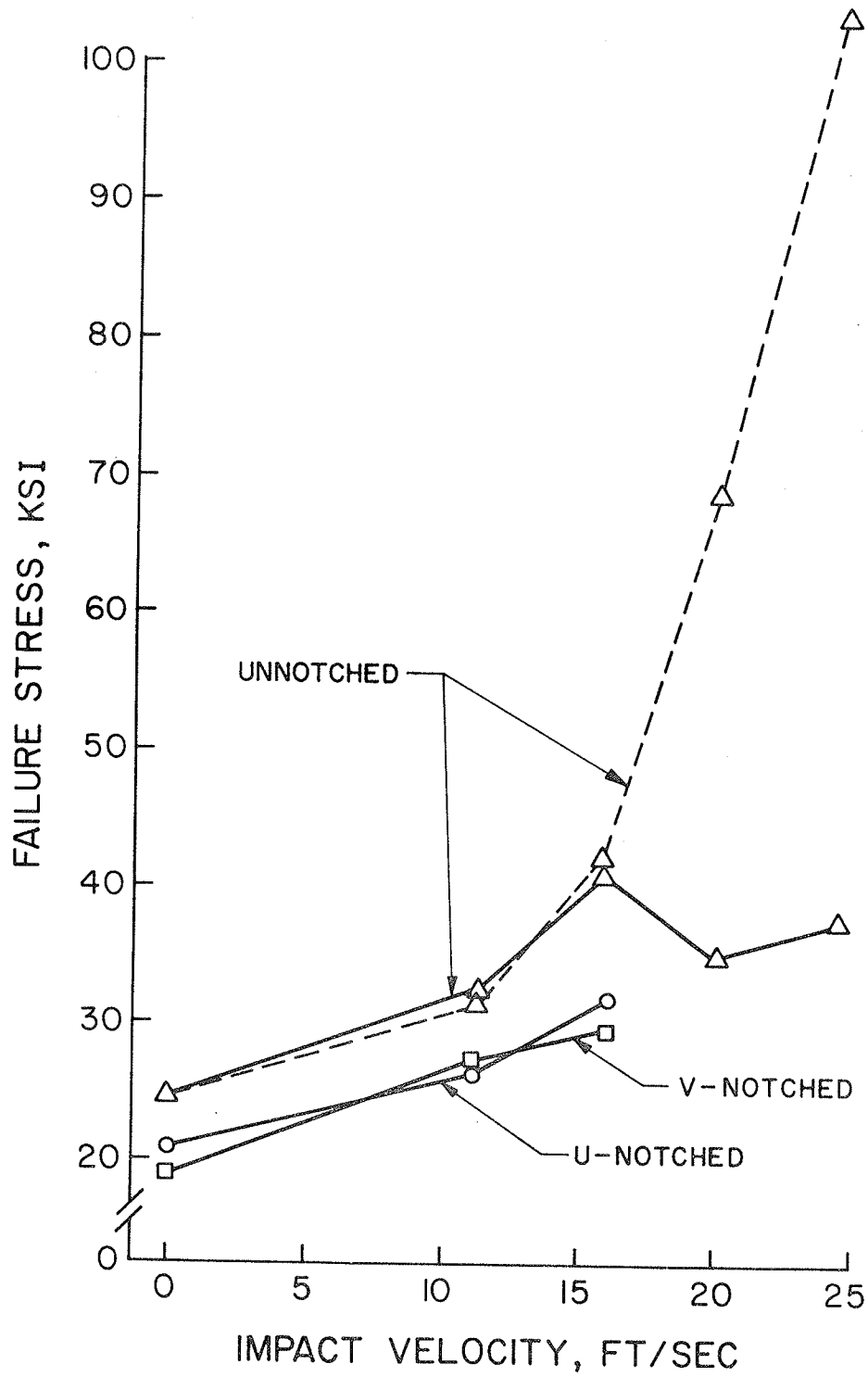


Fig. 21 Loading Rate Effect to the Failure Stress of G20 Specimens

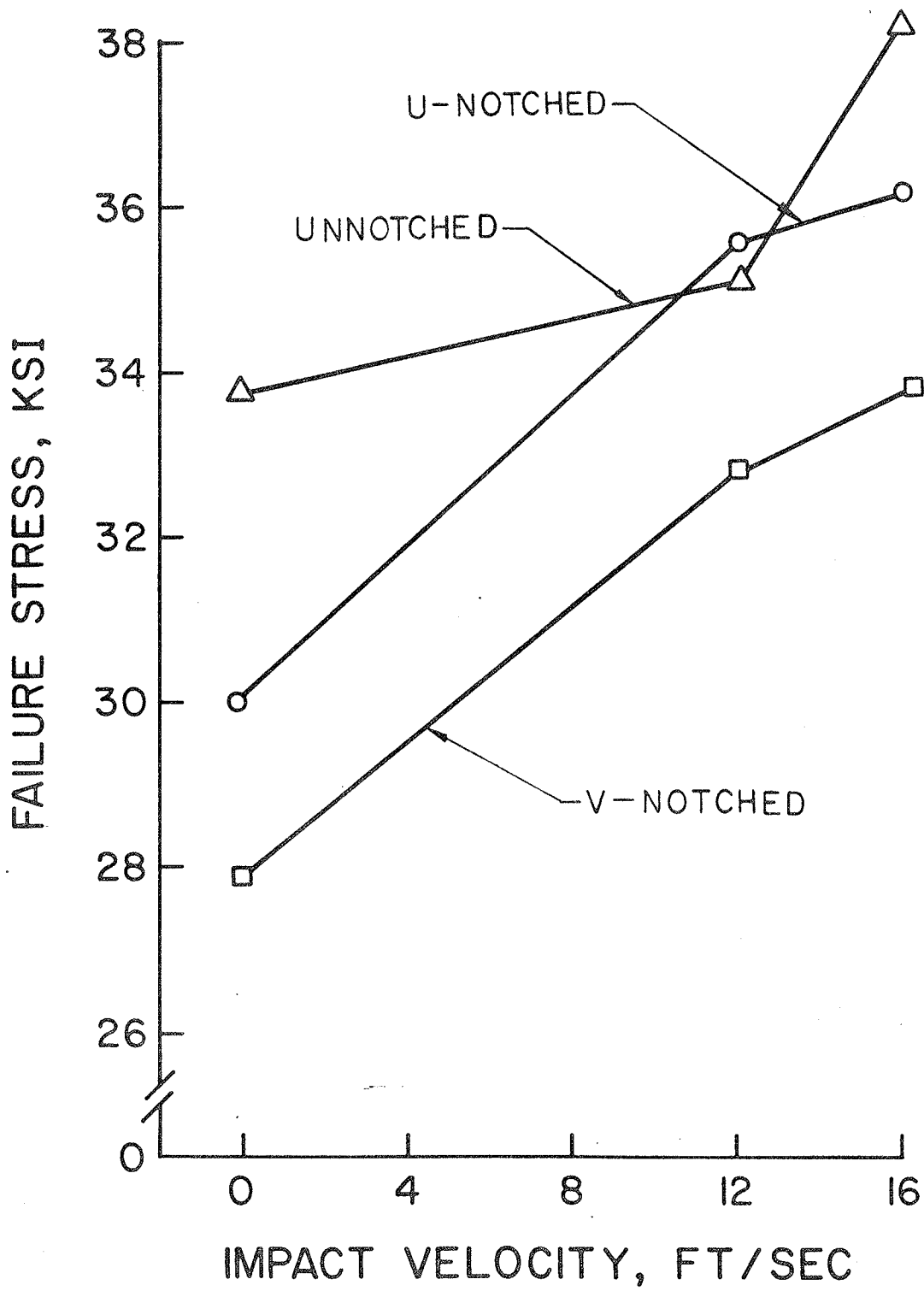


Fig. 22 Loading Rate Effect to the Failure Stress of G40 Specimens

increases, the local plastic deformation of the flake increases. When the stress reaches a level that exceeds the cohesive strength of the matrix, the cracks form. These cracks constitute further stress raisers and the points of maximum stress migrate with the tips of the cracks. Finally as the general level of stress increases with increase of the load and with further decrease of the effective cross-sectional area due to cracks, failure occurs at an average stress very much lower than that corresponding to the strength of the matrix under uniform stress.

It is well known that loading rate sensitivity, or strain-rate sensitivity is a good indicator of the change of deformation behaviours. The local plastic deformation around the graphite flakes of the gray castings could be significantly reduced as the loading rate increases. Less local plastic deformation occurs as the loading rate increases, and therefore a larger load is required to fracture the specimen. Although it was not possible to measure the elongation of the specimens during the impact tests, less deformation of the specimens than that in the static tests was expected.

Gilbert^[5] did a series of impact tests to investigate the loading rate effect on the failure energy of the cast iron material. The results show that the

impact energy value decreases when the impact velocity decreases. Gilbert concluded the test results as follow: "Since plastic deformation is time dependent it is to be expected that increase in the speed of loading would result in a decrease in the amount of plastic deformation. This would tend to lower the impact value (energy) unless there was a substantial increase in the stress of failure". The results of the work done in this thesis might provide a supplemental explanation to Gilbert's results. Though the plastic deformation decreases as the loading rate increases, the energy values could still increase due to the substantial increase in the stress at failure.

5.6 Notch, Size and Grade Effect

Gray cast iron is usually considered as a heterogeneous brittle material. In comparison to ductile materials, it has relatively low notch sensitivity, because even unnotched material is already permeated with internal stress raisers.

The impact test results of the notched specimens show a similar loading rate effect on the failure strength as was shown in the unnotched specimens. This may indicate that notch geometry does not change the nature of the failure of gray cast iron material.

Unnotched G40 specimens with different cross sectional areas were tested. From the data presented in Chapter 4, a greater size effect was observed in the impact tests than that in the static tests. However the number of the tests performed to study size effect was inadequate and the results scattered within relatively wide ranges. The statement of the size effect should be justified by further experimental investigation.

It was found that G20 gray iron showed a greater loading rate dependence on the failure strength than G40 gray cast iron did. It could possibly be explained from the deformability point of view. The additional nickel component of G40 gray iron reduces the size of the graphite flakes, increases the strength and hardness, and simultaneously reduces the deformability of the material. This tends to make G40 gray iron less sensitive to the loading rate effect than G20 gray iron.

CHAPTER 6
CONCLUSIONS

6.1 Conclusions

Supported by a literature survey and the data obtained from the tests described in this thesis, the following conclusions are made:

1. The equipment, in particular the instrumented drop weight testing machine designed and constructed for the experiment is satisfactory for investigating the loading rate effect on the failure strength of gray cast iron within a certain impact velocity range.

2. The failure strength of both the G20 and G40 gray cast iron shows loading rate dependence. The failure strength increases as the loading rate increases. The G20 gray cast iron shows greater loading rate sensitivity than the G40 gray cast iron does.

3. Gray cast iron was found to be essentially notch insensitive under static, as well as impact loading.

6.2 Suggestions for Further Research

The test results presented in this thesis show gray cast iron is a loading rate sensitive material. For more meaningful and accurate results on this aspect, some experimental modification could be made as follows:

1. In order to obtain valid force-time records over a wider range of various loading rates, the test system, in particular the load cell assembly, must be modified by increasing its fundamental frequency.

2. The effort may be made to measure the deformation of the specimens during the impact tests. It will provide load-deformation-time records, giving a more precise description of the properties of the material under dynamic loading.

3. The determination of the correct value of failure stress may depend on the precise measurement of the fundamental frequency of the test system and the time required to fracture the specimen.

4. More tests for each type of loading condition and specimen configuration are strongly suggested.

LIST OF REFERENCE

- (1) ASTM A48-76 Standard Specification for Gray Iron Castings
- (2) ASTM A327-72 "Impact Testing of Cast Iron"
- (3) Metals Handbook: "Properties and Selection of Metals" ASM Vol. 1, 8th Edition.
- (4) Angus: "Cast Iron", Butterworths Publish, London, 1976.
- (5) G. Gilbert: "Impact Testing of Cast Iron" The British Foundryman, Jan. 1961.
- (6) C.F. Walton: "Gray and Ductile Iron Casting Handbook" McGraw Hill, 1971.
- (7) Materials Engineering, Mid-September, 1975, Vol. 8.2 No. 4.
- (8) R.A. Wullaert: "Application of the Instrumented Charpy Impact Test" ASTM STP 466, 1969.
- (9) M.J. May: "Influence of Inertial Load in Instrumental Impact Tests" ASTM STP 466, 1969.
- (10) R.J. Eiber, A.R. Duffy and G.M. McClure: "Significance of the Drop-Weight Tear Test and Charpy V-Notch Impact Test Results" ASTM STP 466, 1969.
- (11) J. Koo: "Size and Strength Rate Effects of Gray Cast Iron" Graduate Thesis, U. of Manitoba, 1980.
- (12) H.M. Hardy and T.O. Kuivinen: "Stress strain Tests on Various Cast Iron Beam Sections" ASTM STP 97, 1916.
- (13) W. Dally: "Experimental Stress Analysis" pp. 409-413, McGraw-Hill, 1965.
- (14) ASTM E208-69 Conducting Drop-Weight Test.
- (15) D.S. Clark, P.E. Duwez: "Discussion of the Forces Acting in Tension Impact Tests of Materials" Proceeding of ASTM p. 245-248, Sep. 1948.

- (16) C.J. Maiden, S.J. Green: "Compressive Stain-Rate Tests on Six Selected Materials at Strain Rates from 10^{-3} to 10^4 IN/IN/Sec" pp. 496-504, Trans. of ASME, Sep. 1966.
- (17) J. Klepaczko: "Effect of Tempering on Quasi-Static and Impact Fracture Toughness and Mechanical Properties fo 5140H Steel" Tech. Report U. of M. Polish Academy of Sciences, Warsaw, Poland.
- (18) T.G. Beckwith, N. Lewis Buck: "Mechanical Measurements" p. 46-77, Addison-Wesley Publishing Co., 1961.
- (19) G. Dieter: "Mechanical Metallurgy" p. 247-288, p. 347-350, McGraw Hill, 1976.
- (20) J. Miklowitz: "Elastic Waves Created During Tensile Fracture" pp. 122-130, ASME J. of Appl. Mech. Vol. 20, 1953.
- (21) P. Craig: "Structural Dynamics" pp. 111-117 John Wiley & Sons, 1980.
- (22) C.H. Mok and J. Duffy: "The Dynamic Stress-Strain Relation of Metals As Determined From Impact Tests" Inter. J. of Mech. Sci. Vol. 657, 1964.

APPENDIX A

Calibration of the Test Equipments

A.1 Calibration of the Instrumented Bar

As described in Chapter 3, the upper one of the two cross bars holding the cylindrical specimen was instrumented as a load cell. Statically, the bending deflection as indicated by the resistance change of the strain gages is directly proportional to the force applied on the center of the bar. In order to obtain the force values by measuring the strain outputs of strain gages, a calibration is required.

The static calibration was carried out on the Baldwin Universal Testing Machine. The instrumented bar was simple supported and was loaded at the center of the span. Fig. 23 shows the results of the calibration.

The strain-load relation of the instrumented bar was further verified by a dead weight test. During the dead weight test, the instrumented bar was loaded with dead weights ranging from 20 to 50 pounds. The results from the test on the Baldwin Universal testing machine and dead weight test were essentially identical.

Since the instrumented bar always functions within the elastic range and the strain rate effect on steel in elastic range is negligible, the use of statically calibrated results in the dynamic test is thought to be acceptable.

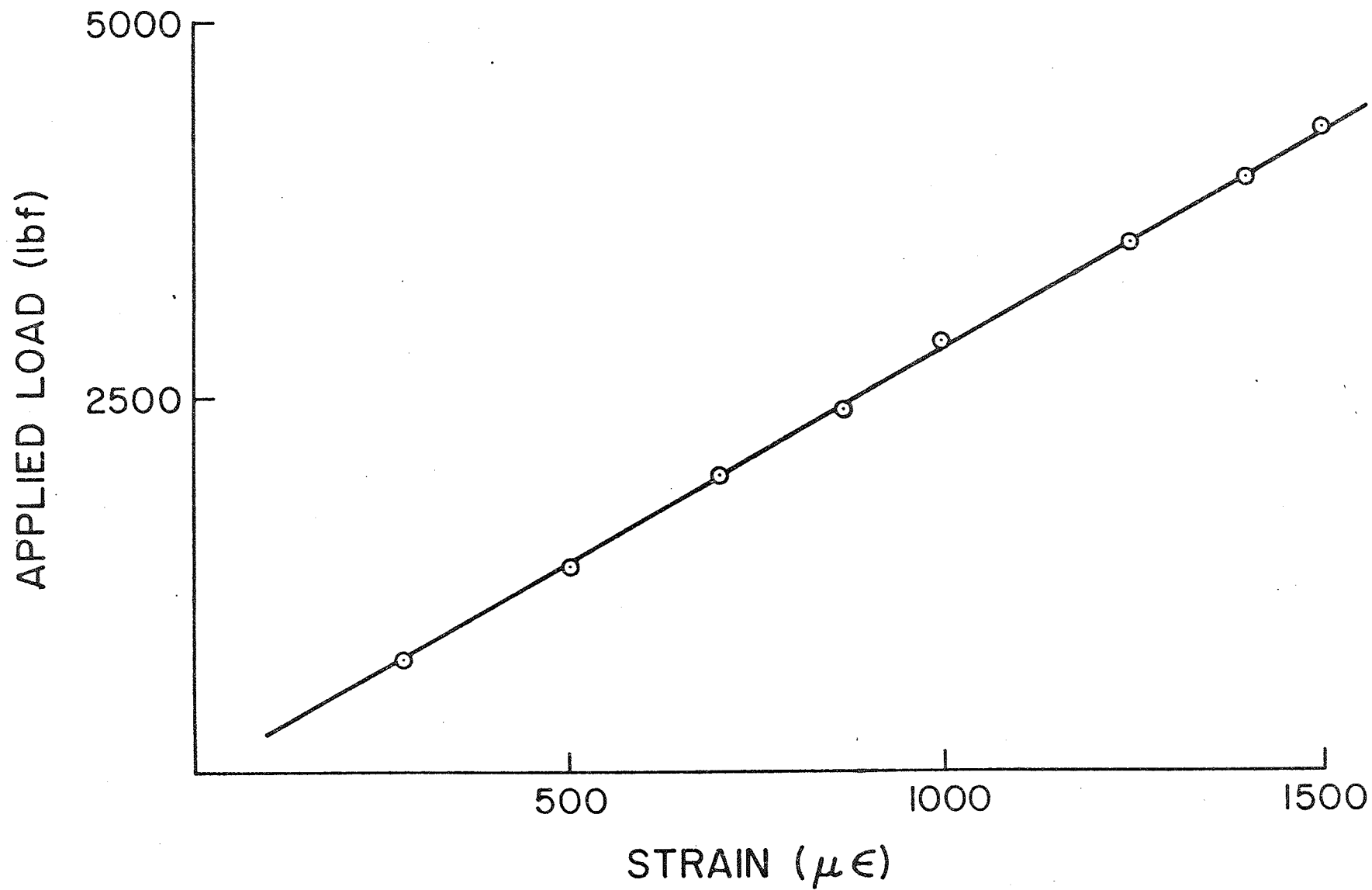


Fig. 23 Calibrated F - ϵ Relation of the Load Cell

A.2 Calibration of the Measurement System

The electronic measurement system includes a amplifier, a waveform recorder and a strip chart recorder. Accurate measurement and recording of the output signal of the strain gages were ascertained by a systematic calibration.

A saw-tooth signal supplied by a function generator was fed to the amplifier-wave form recorder strip chart recorder system. The input signal was chosen to simulate the output signal of the load cell during the impact tests. e.g.

$$\frac{dv}{dt} \text{ saw tooth signal} = \frac{dv}{dt} \text{ output signal of Load Cell at impact test}$$

$$V_{\text{peak}} \text{ saw tooth signal} = V_{\text{peak}} \text{ output signal of Load Cell at Impact Test}$$

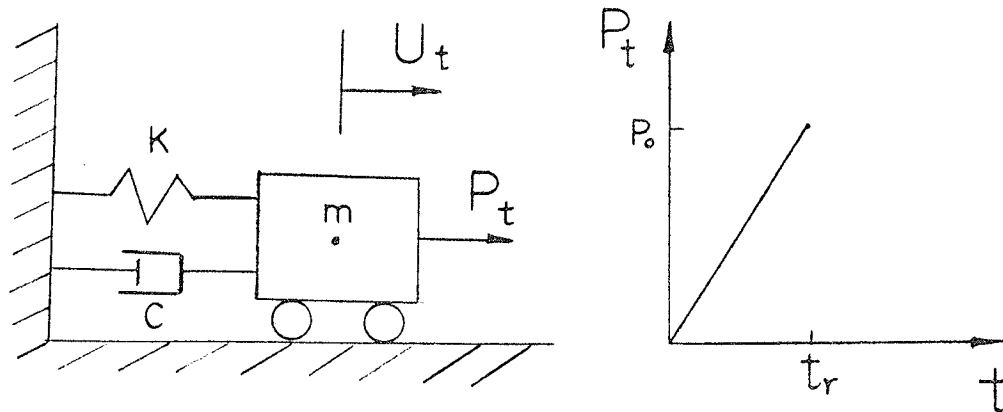
where V - voltage (mv)

t - time (μsec)

The input saw-tooth signal and the output signal of the measurement system were monitored and recorded by a multichannel oscilloscope and a R.M.S. voltmeter. By the comparison of these results it was found that the measurement system has a amplification factor of 78.9 instead of the nominal gain of 100 of the amplifier. There was no significant distortion of the shape of the signal. The good agreement of the outputs from both oscilloscope and voltmeter gives a measure of confidence in the performance of the measurement system.

APPENDIX B

Response of a SDOF System to Ramp Loading



A ramp load with rise time t_r as shown is applied to a damped SDOF system that is at rest prior to application of the load.

The equation of motion and initial conditions are

$$m\ddot{u} + c\dot{u} + ku = \begin{cases} \frac{t}{t_r} P_0 & 0 < t < t_r \\ 0 & t_r < t \end{cases} \dots\dots(1)$$

$$u_0 = \dot{u}_0 = 0$$

where m, c, k - Generalized mass, damping coefficient and stiffness factor respectively.

u - Displacement

t_r - Rising time of ramp load.

For $0 < t < t_r$ (Forced-Vibration Era)

The particular solution is seen to be

$$U_p = \frac{c P_0}{k^2 t_r} + \frac{P_0 t}{k t_r}$$

The complementary solution is given as

$$U_c = e^{-\xi \omega_n t} (A_1 \cos \omega_d t + A_2 \sin \omega_d t)$$

where $\omega_n^2 = \frac{k}{m}$, $\xi = \frac{c}{2k/\omega_n}$

$$\omega_d^2 = \omega_n^2 (1 - \xi^2)$$

Then $U(t) = U_p + U_c$

and with initial conditions $U_0 = \dot{U}_0 = 0$

$$U(t) = e^{-\xi \omega_n t} \left[\frac{CP_0}{k^2 t_r} \cos \omega_d t + \frac{P_0}{k \omega_d t_r} \left(\frac{\xi \omega_n c}{k} - 1 \right) \sin \omega_d t \right] - \frac{CP_0}{k^2 t_r} + \frac{P_0 t}{k t_r}$$

It can also be written in terms of the response ratio R.

$$R(t) = \frac{U(t)}{P_0/k}$$

$$= e^{-2\xi \pi t/T_n} \left[\frac{\xi T_n}{\pi t_r} \cos\left(\frac{2\pi t}{T_n} \sqrt{1-\xi^2}\right) + \frac{(2\xi^2 - 1)T_n}{2\pi \sqrt{1-\xi^2} t_r} \sin\left(\frac{2\pi t}{T_n} \sqrt{1-\xi^2}\right) - \frac{\xi}{\pi} \left(\frac{t}{t_r}\right) + \frac{t}{t_r} \dots \dots \dots (2)\right]$$

$R(t)$ is a function of t , t_n , t_r and ξ .

For $t > t_r$ (Residual-Vibration Era)

The response of SDOF system is free vibration with initial condition $U(t_r)$, $\dot{U}(t_r)$ or $R(t_r)$, $\dot{R}(t_r)$ from expression (2).

The initial conditions for the free vibration era are

$$R_0^* = R(t_r) = e^{-2\pi \xi t_r / r_n} \left[\frac{\xi T_n}{\pi t_r} \cos(2\pi \sqrt{1-\xi^2} \frac{t_r}{T_n}) + \frac{2\xi^2 - 1}{2\pi \sqrt{1-\xi^2}} \cdot \frac{T_n}{t_r} \cdot \sin(2\pi \sqrt{1-\xi^2} \frac{t_r}{T_n}) \right] - \frac{\xi T_n}{\pi t_r} + 1$$

$$\begin{aligned} \dot{R}_o^* = \dot{R}(t_r) = & -\frac{2\pi\xi}{T_n} e^{-2\pi\xi t_r/T_n} \left[\frac{\xi T_n}{\pi t_r} \cos\left(2\pi\sqrt{1-\xi^2} \frac{t_r}{T_n}\right) + \right. \\ & \left. \frac{2\xi^2 - 1}{2\pi\sqrt{1-\xi^2}} \cdot \frac{T_n}{t_r} \sin\left(2\pi\sqrt{1-\xi^2} \frac{t_r}{T_n}\right) \right] + e^{-2\pi\xi t_r/T_n} \left[-\frac{2\xi\sqrt{1-\xi^2}}{t_r} \cdot \right. \\ & \left. \sin\left(2\pi\sqrt{1-\xi^2} \frac{t_r}{T_n}\right) + \frac{2\xi^2 + 1}{t_r} \cos\left(2\pi\sqrt{1-\xi^2} \frac{t_r}{T_n}\right) \right] + \frac{1}{t_r} \end{aligned}$$

where R^* and \dot{R}^* are the response ratio and its time derivative in residual vibration era.

The equation of residual vibration (free vibration) of SDOF is:

$$m\ddot{u} + c\dot{u} + ku = 0$$

where u is displacement during residual vibration era.

Using definition of $R^* = \frac{u}{P_o/k}$, and R_o^* and \dot{R}_o^* , the final solution of the residual vibration can be expressed as

$$\begin{aligned} R^*(t) = e^{-\frac{2\pi\xi t}{T_n}} \left[R_o^* \cos\left(2\pi\sqrt{1-\xi^2} \frac{t}{T_n}\right) + \frac{\dot{R}_o^* T_n + 2\xi\pi R_o^*}{2\pi\sqrt{1-\xi^2}} \cdot \right. \\ \left. \sin\left(2\pi\sqrt{1-\xi^2} \frac{t}{T_n}\right) \right] \dots \dots \dots (3) \end{aligned}$$

(2) and (3) are the solutions of equation (1) during forcing and residual vibration eras respectively.

A numerical evaluation of expression (2) and (3) was performed by a digital computer. The plot of the results is previously shown in Fig. 19.